(54) **Title:** ISOMOTIVE DIELECTROPHORESIS FOR DIELECTRIC ANALYSIS OF PARTICLE SUB-POPULATIONS

FIG. 1

(57) **Abstract:** Provided herein are a methods of analyzing particles and isomotive dielectrophoresis devices, and methods of forming dielectrophoresis devices. The method of analyzing particles includes providing an isomotive dielectrophoresis device; positioning a sample within the device, the sample including at least one particle; applying an electric field to the device, the electric field inducing a constant dielectrophoresis force on the at least one particle of the sample; and monitoring a translation of the at least one particle. One isomotive dielectrophoresis device includes a first electrode having a first surface geometry; a second electrode having a second surface geometry; and an electrically insulating material at least partially surrounding the first electrode and the second electrode.

ISOMOTIVE DIELECTROPHORESIS FOR DIELECTRIC ANALYSIS OF PARTICLE SUB-POPULATIONS

RELATED APPLICATIONS

[0001] This application claims priority from U.S. Provisional Application Serial No. 62/359,850, filed July 8, 2016, and U.S. Provisional Application Serial No. 62/393,391, filed September 12, 2016, the entire disclosures of which are incorporated herein by this reference.

TECHNICAL FIELD

[0002] The presently-disclosed subject matter generally relates to methods and devices for particle analysis. In particular, certain embodiments of the presently-disclosed subject matter relate to methods and devices for isomotive dielectrophoresis (isoDEP) particle analysis.

GOVERNMENT INTEREST

[0003] This invention was made with government support under grant numbers 1550509 and 1560235 awarded by the National Science Foundation (NSF). The government has certain rights in the invention.

BACKGROUND

[0004] The movement of a charged particle within a DC field is called "electrophoresis." Dielectrophoresis (DEP) is the translation of a polarizable particle by applied non-uniform electric fields. Unlike electrophoresis, particles do not need to carry a charge in DEP. The polarization of a particle with DEP is based, in part, on the interfacial polarization at the interface of the liquid/particle boundary under an applied electric field. Selectivity of DEP sorting occurs due to differences in the particles' dielectric properties (conductivity, permittivity) and resultant polarization when subjected to an electric field. This selectivity may be used to either attract or repel the particles from regions of greater field strength. For example, an AC field is typically used for dielectrophoresis to either (i) mitigate electrophoretic movement and/or (ii) translate negligibly charged neutral particles.

[0005] Through particle manipulation, DEP has been able to capture, sort, concentrate, and characterize a variety of particles and biological entities as small as a few nanometers. The polarization behavior of a particle observed over a spectrum of AC frequencies also provides insight into its state and composition, a characteristic utilized in electrorotation. Thus, an important characteristic of DEP is that by tracking the magnitude and direction of manipulated particles' velocities over a range of applied AC frequencies, the dielectric properties of the particles can be extracted and subsequently used for

particle identification or analysis. For example, DEP has been used to differentiate subpopulations of cells including live and dead bacteria, healthy and damaged phytoplankton, breast cancer sublines, circulating tumor cells from non-transformed cells, leukocyte subpopulations (T lymphocytes, B lymphocytes, granulocytes, monocytes), and blood types.

[0006] However, from the perspective of particle analysis, the primary disadvantage of current dielectrophoretic systems is that the applied DEP force is spatially non-uniform, especially in three dimensions, which complicates or prevents comprehensive cellular sub-population analysis. In contrast to a uniform field, where the net dielectrophoretic force on the particle is zero, DEP requires a non-uniform electric field to provide a non-zero net force on the particle. The magnitude of the DEP force is a proportional to the gradient of the field-squared (∇E_{rms}^2) and, therefore, is highly dependent on the electrode geometry and layout. The most prevalent DEP systems use co-planar metal electrodes. In these planar designs, the DEP force is inherently greatest close to the surface of the electrodes, but exponentially decreases with height above the electrode plane. Therefore, samples are exposed to highly non-uniform DEP forces. For example, using co-planar electrodes with a 25 μm gap, the magnitude of the DEP force is approximately 100 times greater for a particle 1 μm above the electrode edge compared to when it is 10 μm away – a distance comparable to the diameter of some biological cells.

[0007] Additionally, there are several electrohydrodynamic phenomena that may deter the operation of DEP devices, namely AC electro-osmosis (ACEO) and electrothermal (ET) flow. ACEO occurs when the electric field acts upon the charges accumulated on the surface of a polarized electrode, inducing hydrodynamic slip. In general, ACEO increases at lower AC frequencies, becomes negligible at high fluid conductivities, is a function of electrolyte type, and is proportional to E^2. ET flow is generated when the electric field acts upon dielectric gradients (permittivity, conductivity) in the fluid. These dielectric gradients are generated through non-uniform heating via Joule heating or external heating sources. ET flow is proportional to E^2 (external heating) or E^4 (Joule heating) and becomes negligible at high AC frequencies; ET flow can be reduced through proper heat transfer design to eliminate regions of large temperature gradients. Joule heating in electrokinetic chips is proportional to E^2 and the conductivity of the media (σ). Joule heating can been avoided by using low conductivity media (< 1.0 S/m).

[0008] In view of the challenges and/or disadvantages discussed above, most DEP applications focus on trapping, manipulating, or sorting particles, not particle analysis. That said, to address these issues, several designs have been used to more effectively distribute DEP forces, including placing electrodes on the top and bottom of the channel and 3D electrode fabrication. However, 3D electrode fabrication is nontrivial and typically requires complex microfabrication equipment and/or facilities. Other techniques that utilize glass/polymer structures, namely insulator-based DEP and contactless DEP, typically require relatively large voltages (> 100 V). These relatively large voltages may lead to

unwanted electrokinetic effects that can induce device dielectric breakdown or disturb biological samples. Further, a previous study generated a relatively constant DEP force within an insulative microchannel constriction, though analysis was restricted to a specific channel region. Therefore, while non-uniform forces may be suitable for sorting applications, a constant DEP force field would simplify analysis where resultant dielectric properties could be determined from analyzing particle trajectories.

[0009] An alternate technique includes electrorotation (ROT). Cellular ROT involves the use of rotating fields generated, typically, by a four-electrode system that are designed to isolate single cells (**FIG. 1**, left). The direction and rate of particle spin is a function of the field spatial configuration and its AC frequency as well as the dielectric properties of the media and cell. ROT can discriminate dielectric differences between single cells and has been used to differentiate cells with different morphologies and other biological characteristics (**FIG. 1**, right).

[0010] ROT systems provide detailed electrokinetic measurements of cell subpopulations, though its most significant disadvantage is its limited throughput which results from its inherent design of trapping and analyzing individual cells (**FIG. 1**, left). For example, Han, et al. used ROT to differentiate between six cell types but acquired ROT data using an average of *nine* cells for each cell type (54 cells total). Further, the physics of laminar microfluidic flows makes it nontrivial to position individual cells within an electrode region whose geometry is on the same scale as the diameter of the cell (**FIG. 1**, left). Analyzing a larger cell subpopulation will provide additional insight into how that specific cell type is affected by external stimuli (e.g., environmental factors).

[0011] Other techniques for cell subpopulation analysis include flow cytometry and electrical impedance spectroscopy (EIS). Flow cytometry is a laser-based technique used for cell counting, cell sorting, and biomarker detection that can process thousands of cells per second. Scattered light is detected from a fluorescently labeled cell as it passes through a laser beam (or multiple beams). Specialized software analyzes collected data to determine cell size, internal properties, phenotype, etc. One of the primary benefits is that flow cytometry enables simultaneous measurements of different cell characteristics as several labels could be applied to the sample population. However, disadvantages include (i) the high cost of flow cytometers, (ii) the complexity of its operation, usually requiring a trained technician to operate, (iii) the large, bulky size of flow cytometry systems, and (iv) the time/cost associated with the application of fluorescent labels to the sample. Therefore, flow cytometry systems are found in a relatively small number of universities and scientific research centers and seldom used in remote/portable research applications.

[0012] Label-free single cell characterization is possible using EIS. EIS allows the quantitative measurement of the inherent electrical and dielectric properties of cells and can be integrated with other lab-on-a-chip technologies. EIS systems measure the electrical impedance of cells at a particular AC frequency. There are two types of EIS systems, dynamic and static. Dynamic EIS systems provide

3

higher throughput, although they also have limited sensitivity (i.e., measurements are typically acquired at one specific AC frequency). Static EIS systems trap individual cells and obtain detailed impedance spectra (i.e. over a range of AC frequencies) of the cell enabling highly sensitive measurements. However, static EIS systems have limited throughput since detailed spectra take additional measurement time and require cell isolation. Furthermore, static EIS systems require more sophisticated equipment (i.e. expensive impedance analyzers like Agilent 4294A, $47,500) to perform impedance measurements across a broad range of AC frequencies.

[0013] As such, any improvements to the articles and methods for the analysis of cell subpopulations would be both highly desirable and beneficial.

SUMMARY

[0014] The presently-disclosed subject matter meets some or all of the above-identified needs, as will become evident to those of ordinary skill in the art after a study of information provided in this document.

[0015] This summary describes several embodiments of the presently-disclosed subject matter, and in many cases lists variations and permutations of these embodiments. This summary is merely exemplary of the numerous and varied embodiments. Mention of one or more representative features of a given embodiment is likewise exemplary. Such an embodiment can typically exist with or without the feature(s) mentioned; likewise, those features can be applied to other embodiments of the presently-disclosed subject matter, whether listed in this summary or not. To avoid excessive repetition, this summary does not list or suggest all possible combinations of such features.

[0016] Provided herein, in some embodiments, is a method of analyzing particles, comprising providing an isomotive dielectrophoresis device; positioning a sample within the device, the sample including at least one particle; applying an electric field to the device, the electric field inducing a constant dielectrophoresis force on the at least one particle of the sample; and monitoring a translation of the at least one particle. In one embodiment, the at least one particle includes a cell. In another embodiment, positioning the sample within the device comprises injecting the sample into the device until bulk fluid motion is halted. In a further embodiment, the constant dielectrophoresis force comprises a constant force within an analytical space of the device.

[0017] In some embodiments, applying the electric field to the device comprises applying an AC signal across a channel in the device. In one embodiment, the AC signal is between 100 Hz to 100 MHz, 1 kHz and 100 MHz, 1 kHz and 50 MHz, 1 kHz and 10 MHz, or any suitable combination, sub-combination, range, or sub-range thereof. In some embodiments, applying the electric field to the device comprises applying an AC signal through a channel in the device. In some embodiment, the method further comprises extracting dielectric properties of the at least one particle. In some

4

embodiments, the method further comprises determining a cell physiology from the dielectric properties.

[0018] Also provided, in some embodiment, is an isomotive dielectrophoresis device, comprising a first electrode having a first surface geometry; a second electrode having a second surface geometry; and an electrically insulating material at least partially surrounding the first electrode and the second electrode. The first electrode and the second electrode are arranged and disposed to provide a constant dielectrophoresis force within an analytical space of the device. In one embodiment, the first electrode and the second electrode are arranged and disposed to provide a constant gradient field-squared within the analytical space of the device. In another embodiment, the first electrode and the second electrode define a microchannel therebetween. In a further embodiment, the constant dielectrophoresis force is applied across the microchannel. In some embodiments, the analytical space of the device comprises a portion of the microchannel.

[0019] In one embodiment, a method of forming the isomotive dielectrophoresis device comprises selecting a curvature of the first electrode and a curvature of the second electrode based upon the equation $V = \frac{2}{3}kr^{3/2}sin\left(\frac{3\theta}{2}\right)$.

[0020] Further provided, in some embodiments, is an isomotive dielectrophoresis device comprising a first insulative feature having a first surface geometry, a second insulative feature having a second surface geometry, and at least one electrode positioned upstream and at least one electrode positioned downstream of an analytical space. The first insulative feature and the second insulative feature are arranged and disposed to form a microchannel extending from the inlet to the outlet of the device, and the first surface geometry of the first insulative feature and second surface geometry of the second insulative feature are arranged and disposed to provide a constant dielectrophoresis force within an analytical space of the device. In one embodiment, the first electrode and the second electrode are arranged and disposed to provide a constant electrical field gradient within the analytical space of the device. In another embodiment, the constant dielectrophoresis force is applied through the microchannel. In a further embodiment, the analytical space of the device comprises a portion of the microchannel.

[0021] In one embodiment, a method of forming the isomotive dielectrophoresis device comprises selecting a curvature of the first electrode and a curvature of the second electrode based upon the equation $V = \frac{2}{3}kr^{3/2}cos\left(\frac{3\theta}{2}\right)$.

[0022] Further features and advantages of the presently-disclosed subject matter will become evident to those of ordinary skill in the art after a study of the description, figures, and non-limiting examples in this document.

BRIEF DESCRIPTION OF THE DRAWINGS

[0023] FIG. 1 shows an image of a typical four-electrode electrorotation (ROT) system (left) and a graph illustrating a sample spectra demonstrating subpopulation differentiation of six cell types (right).

[0024] FIG. 2 shows a multilayered spherical model with labeled dielectric properties of the liquid solution (s), membrane (m), and cytoplasm (c) (left) and associated $Re[K_{CM}]$ and $Im[K_{CM}]$ spectra.

[0025] FIGS. 3A-E show graphs and images of an electrode-based isomotive dielectrophoresis system according to an embodiment of the disclosure. **(A)** shows an electrode geometry for isoDEP force. For the shown electrode geometry, a value of $\nabla E_{rms}^2 = 6.8 \times 10^{11}$ V^2/m^3 will be produced for an applied potential of 10 V. **(B)** shows an electrode-based isoDEP system using extruded two-dimensional electrodes, with the respective equipotential lines (solid lines) and electric field lines (dashed lines) illustrated therein. **(C)** shows an electric field being applied across the microchannel of an electrode-based isoDEP system. **(D)** shows a cross-section view of the isoDEP system of **FIGS. 3A-C**. **(E)** shows a picture of a fabricated microelectrode isoDEP device including two electrodes with $r_{60,1} = 77$ μm and $r_{60,2} = 577$ μm.

[0026] FIGS. 4A-E show graphs and images of an insulator-based isomotive dielectrophoresis system according to an embodiment of the disclosure. **(A)** shows an isoDEP system using insulative microchannel curvature, with the respective equipotential lines (solid lines) and electric field lines (dashed lines) illustrated therein. **(B)** shows a schematic view of a Su-8 mold geometry with $r_{60,1} = 77$ μm and $r_{60,2} = 577$ μm. The experimental observation area is shown as well as how the AC signal was applied. **(C)** shows an electric field being applied through the channel. **(D)** shows a cross-section view of the isoDEP system of **FIGS. 4A-C** with electrodes at the fluid inlet and outlet of the system, according to an embodiment of the disclosure. **(E)** shows a cross-section view of the isoDEP system including electrodes embedded upstream and downstream of the analytical space, according to an embodiment of the disclosure.

[0027] FIG. 5 shows that the magnitude of velocity that a particle undergoes during dielectrophoresis is a function of its dielectric properties. It is either repelled from the 'origin' of the device (positive DEP) or attracted towards the device (negative DEP). For either case, particle translation moves radially to/from the origin. r_{60} refers to the distance from the origin to the respective curve at $\theta = 60°$ and L is the distance between the origin and the electrode. The theoretical isoDEP radial trajectory of a nDEP and pDEP particle is shown.

[0028] FIG. 6 is a schematic view of an isoDEP process including injecting a sample, applying a field, and acquiring an image.

[0029] FIGS. 7A-C show images illustrating fabrication of an isoDEP system. **(A)** shows a top view of features milled into a copper sheet. **(B)** shows the sheet subsequently plated with nickel/gold and diced. **(C)** shows the metal sheet sealed between two acrylic substrates, one containing fluid access

ports. General-use epoxy and conductive epoxy will be used to seal the microchannels and create electrical connections, respectively.

[0030] **FIG. 8** shows 8 μm polystyrene particles trapped in a 3D quadropole electrode machined with a 100 μm bit.

[0031] **FIG. 9** is Photolithographic mask for the fabrication of proof-of-concept isomotive DEP devices. The red lines denote final device dimensions of approximately 11.0 mm x 11.0 mm. The yellow areas denote the regions that will be etched via deep reactive ion etching (DRIE). The grid in the figure provides a 5.0 mm scale.

[0032] **FIGS. 10A-B** shows images of isoDEP devices according to an embodiment of the disclosure. (**A**) shows diced 4" wafer illustrating the final isomotive DEP devices. (**B**) shows an individual device with two identical channels next to a penny for scale.

[0033] **FIGS. 11A-B** shows images demonstrating consistent radial translation of particles in an isoDEP device. (**A**) shows radial translation using polystyrene particles exhibiting negative DEP (overlaid particle images are 1.25 seconds apart). (**B**) shows radial translation using silver-coated particles exhibiting positive DEP (overlaid particle images are 0.67 seconds apart).

[0034] **FIGS. 12A-B** show images illustrating the path of individual particles undergoing nDEP towards the origin. (**A**) shows the path of individual particles (n = 110) undergoing nDEP towards the origin at 100 kHz, 15 V. (**B**) shows a linear fit for each respective path. (r_{60} = 0.5mm).

[0035] **FIGS. 13A-B** show images of particle scaled velocity and trajectory. (**A**) shows a comparison of a particle's scaled velocity (V_{DEP}/a^2) with the average of the group (n = 110). (**B**) shows the angle at which the particle's trajectory deviates from the theoretical direction (i.e., pure radial trajectory).

[0036] **FIGS. 14A-B** show images illustrating negative and positive DEP with an insulative isoDEP device according to an embodiment of the disclosure. (**A**) shows negative DEP with the insulative isoDEP device at 300 V and 2 kHz. (**B**) shows positive DEP with the insulative isoDEP device at 300 V and 2 kHz. Polystyrene particles were used in (**A**) with overlaid particle images 2.0 seconds apart. Silver-coated hollow glass particles were used in (**B**) with overlaid particle images 0.33 seconds apart. The image insert in (**B**) shows pearl chaining in the direction of the applied electric field.

[0037] **FIG. 15** shows the path of individual particles (n = 18) undergoing negative DEP translation towards the origin over a period of 2.0 seconds at 300 V and 2 kHz. The dashed line denotes a 120° angle with the system origin labeled with a black circle.

DESCRIPTION OF EXEMPLARY EMBODIMENTS

[0038] The details of one or more embodiments of the presently-disclosed subject matter are set forth in this document. Modifications to embodiments described in this document, and other

embodiments, will be evident to those of ordinary skill in the art after a study of the information provided in this document. The information provided in this document, and particularly the specific details of the described exemplary embodiments, is provided primarily for clearness of understanding and no unnecessary limitations are to be understood therefrom. In case of conflict, the specification of this document, including definitions, will control.

[0039] While the terms used herein are believed to be well understood by those of ordinary skill in the art, certain definitions are set forth to facilitate explanation of the presently-disclosed subject matter.

[0040] Unless defined otherwise, all technical and scientific terms used herein have the same meaning as is commonly understood by one of skill in the art to which the invention(s) belong.

[0041] All patents, patent applications, published applications and publications, GenBank sequences, databases, websites and other published materials referred to throughout the entire disclosure herein, unless noted otherwise, are incorporated by reference in their entirety.

[0042] Where reference is made to a URL or other such identifier or address, it understood that such identifiers can change and particular information on the internet can come and go, but equivalent information can be found by searching the internet. Reference thereto evidences the availability and public dissemination of such information.

[0043] Although any methods, devices, and materials similar or equivalent to those described herein can be used in the practice or testing of the presently-disclosed subject matter, representative methods, devices, and materials are described herein.

[0044] The present application can "comprise" (open ended) or "consist essentially of" the components of the present invention as well as other ingredients or elements described herein. As used herein, "comprising" is open ended and means the elements recited, or their equivalent in structure or function, plus any other element or elements which are not recited. The terms "having" and "including" are also to be construed as open ended unless the context suggests otherwise.

[0045] Following long-standing patent law convention, the terms "a", "an", and "the" refer to "one or more" when used in this application, including the claims. Thus, for example, reference to "a cell" includes a plurality of such cells, and so forth.

[0046] Unless otherwise indicated, all numbers expressing quantities of ingredients, properties such as reaction conditions, and so forth used in the specification and claims are to be understood as being modified in all instances by the term "about". Accordingly, unless indicated to the contrary, the numerical parameters set forth in this specification and claims are approximations that can vary depending upon the desired properties sought to be obtained by the presently-disclosed subject matter.

[0047] As used herein, the term "about," when referring to a value or to an amount of mass, weight, time, volume, concentration or percentage is meant to encompass variations of in some embodiments ±20%, in some embodiments ±10%, in some embodiments ±5%, in some embodiments ±1%, in some

embodiments ±0.5%, and in some embodiments ±0.1% from the specified amount, as such variations are appropriate to perform the disclosed method.

[0048] As used herein, ranges can be expressed as from "about" one particular value, and/or to "about" another particular value. It is also understood that there are a number of values disclosed herein, and that each value is also herein disclosed as "about" that particular value in addition to the value itself. For example, if the value "10" is disclosed, then "about 10" is also disclosed. It is also understood that each unit between two particular units are also disclosed. For example, if 10 and 15 are disclosed, then 11, 12, 13, and 14 are also disclosed.

[0049] As used herein, "optional" or "optionally" means that the subsequently described event or circumstance does or does not occur and that the description includes instances where said event or circumstance occurs and instances where it does not. For example, an optionally variant portion means that the portion is variant or non-variant.

[0050] As used herein, "polarizable particle" means a particle that forms concentrations of charge when subjected to a field. One example includes the formation of a dipole (two poles of charge) in the direction of the field. These poles form at the interface between the particle/fluid.

[0051] The presently-disclosed subject matter describes analytical devices and methods that provide advantages over existing DEP devices and other technologies. For example, in some embodiments, the devices and methods include electrokinetic analysis that provides detailed dielectric measurements of individual cells. In one embodiment, the detailed dielectric measurements of individual cells facilitate and/or provide identification of cell sub-populations. In another embodiment, the detailed dielectric measurements of individual cells facilitate and/or provide measurement of variants within a cell population.

[0052] In some embodiments, the presently-disclosed subject matter includes a method of generating a constant dielectrophoretic (DEP) force. The time-averaged dielectrophoretic force of a homogeneous spherical particle is:

$$\bar{F}_{DEP} = 2\pi\varepsilon_m a^3 Re[K_{CM}]\nabla E_{rms}^2 \tag{1}$$

where ε is permittivity and the subscript m refers to fluid medium properties, a is the particle radius, $\bar{E}_{rms}$ is the root mean square electric field, and the term K_{CM} refers to the Clausius-Mossotti factor, which is defined as:

$$K_{CM} = \left(\varepsilon_p^* - \varepsilon_m^*\right)/\left(\varepsilon_p^* + 2\varepsilon_m^*\right) \tag{2}$$

where the subscript p refers to particle properties. The complex permittivity ε^* is given by

$$\varepsilon^* = \varepsilon - j\sigma/(\omega) \tag{3}$$

where σ is conductivity, $\omega = 2\pi f$, f is the AC frequency, and j is $\sqrt{-1}$.

[0053] According to Equation (1), a particle's resultant DEP motion is a function of particle radius (known or measured optically using established methods), Clausius-Mossotti factor (a function of the applied AC frequency, fluid conductivity, fluid permittivity, particle conductivity, and particle permittivity), and gradient of electric field squared (∇E_{rms}^2). The Clausius-Mossotti factor is assumed unknown, can be measured through quantifying particle translation, is different for various cell and particle types (conductive vs insulative, live vs dead, cancerous vs noncancerous, etc.), and a detailed frequency sweep can provide detailed insight into cell/particle composition and/or state (e.g., compromised cell membrane). The gradient of electric field squared is assumed known from electrode geometry.

[0054] The DEP force in Equation (1) also assumes that the particle is spherical and homogeneous. However, in some embodiments, Equation (1) may be modified for multi-shelled and non-spherical particles which can be used to describe biological particles. For example, refer to the multilayered spherical model in **FIG. 2** with labeled dielectric properties of the liquid solution (s), membrane (m), and cytoplasm (c). DEP and ROT experimentation can yield $Re[K_{CM}]$ and $Im[K_{CM}]$ spectra (arbitrary representative curves shown in **FIG. 1**). The spectra is shifted with changes in cell morphology (ex: membrane thickness) and dielectric properties (ε, σ). For example, a dead cell may have a leaky membrane such that the cytoplasm is released – such changes can be identified with these spectra. Such cell dielectric characteristics can be extracted from fitting acquired measurements to an assumed geometrical cell model.

[0055] Particle shape aside, the dielectrophoretic force is dependent on the real part of the Clausius-Mossotti factor and governs the attraction or repulsion of particles from regions of high field strength. If $Re[K_{CM}]$ is negative, the particle experiences negative DEP (nDEP) and is repelled from larger field regions; vice versa for a positive value of $Re[K_{CM}]$, when a particle experiences positive DEP (pDEP) it is attracted to high field regions. In one embodiment, the range of values for $Re[K_{CM}]$ is between +1 and -0.5. In another embodiment, the experimentally altering the medium changes the direction of DEP.

[0056] Following the discussion above, in some embodiments, generating an isomotive dielectrophoretic (DEP) force includes providing a potential according to one of the following forms (in cylindrical coordinates):

$$V = {}^2\!/_3\, k\, r^{3/2} \sin(3\theta/2) \qquad\qquad (4a)$$

$$V = {}^2\!/_3\, k_i\, r^{3/2} \cos(3\theta/2) \qquad\qquad (4b)$$

where k and k_i are constants for the microelectrode and insulative platforms, respectively. From this, the following equation is derived:

$$\|E_{rms}\| = k\, r^{1/2} \quad \rightarrow \quad \nabla\!\left(E_{rms}{}^2\right) = k^2 \hat{r} \qquad\qquad (5)$$

(the insulative case will yield the same result using k_i instead of k). Therefore, the gradient of the field-squared, and thus the DEP force, is constant between any two equipotential lines that follow Eq. (4). The resultant force is applied in the radial direction.

[0057] Also provided, in some embodiments of the presently-disclosed subject matter, are isomotive dielectrophoresis (isoDEP) systems arranged and disposed to provide isomotive dielectrophoresis (isoDEP). In one embodiment, isoDEP refers to a dielectrophoretic device where the dielectric properties of particles (e.g., cells) are extracted from particle tracking or particle velocimetry measurements. For example, in another embodiment, an electric field is applied and polarizable particles with negligible net charge are translated due to dielectrophoresis (DEP), or the translation of particles in a non-uniform field. In a further embodiment, as illustrated in **FIGS. 3A-4E**, the isoDEP devices and/or methods described herein apply a uniform DEP force to all particles within the optical viewing area, providing uniform (isomotive) microparticle translation.

[0058] In contrast to existing DEP devices and/or methods, the isoDEP systems disclosed herein generate an electric field such that the induced DEP force is constant for all particles within the optical viewing area (i.e., analytical space). In one embodiment, from straightforward particle tracking throughout the isoDEP region, the applied DEP force can be measured and the dielectric properties of individual particles can be obtained. In another embodiment, several AC frequencies can be applied to acquire a comprehensive dielectric response.

[0059] In certain embodiments, isoDEP is accomplished through a unique geometry where the gradient of the field-squared (∇E_{rms}^2) is constant. In some embodiments, applying a uniform DEP force includes arranging and disposing one or more electrodes to apply the uniform DEP force. In one embodiment, the electrodes are configured to provide a constant value of ∇E_{rms}^2 in the viewing area when an electric field is applied thereto. In another embodiment, as illustrated in **FIGS. 3A-E**, in contrast to the two-dimensional isomotive DEP solution suggested by Herbert Pohl, the isoDEP devices described herein include a three-dimensional electrode geometry. Additionally, while Pohl describes a two-dimensional solution for particle sorting, which requires continuous fluid flow, in some embodiments, the presently-disclosed subject matter provides individual particle analysis where a flow of the sample is stopped during an analysis period.

[0060] The three-dimensional electrode geometry includes any suitable geometry and/or profile capable of providing a constant DEP force within a desired analytical space. For example, **FIGS. 3A-B** illustrate two curves representing equipotential boundaries to an isomotive field solution, where Equation (4a) represents the equation of each line of voltage, V. As illustrated in **FIG. 3B**, the resultant electric field (dashed lines) produces a constant gradient of the field squared, according to Equation (5). In some embodiments, this uniform electric field is applied between the electrodes and across the

microchannel formed therebetween (**FIG. 3C**). Therefore the DEP force is constant in the region between two such boundaries.

[0061] Suitable geometries and/or profiles include, but are not limited to, straight-walled, curved, rounded, angled, oblique, or a combination thereof. Additionally, opposing surfaces of the one or more electrodes may include the same, substantially the same, or different geometrical shapes and/or sizes. For example, referring again to **FIGS. 3A-B**, the surface of one electrode includes two flat or substantially flat portions intersecting at an obtuse angle while an opposing surface of another electrode includes a curved geometry substantially corresponding to the angle of the surface of the first electrode. The curvature of the two electrodes follows the profile defined in Equation 5. Additionally, in some embodiments, a ground electrode (V = 0; **FIG. 3B**) following a 120° angle with the system's origin at its bend is provided. These three-dimensional electrodes are contained by electrically insulating material, such as glass, and provide a two-dimensional field throughout the depth of a chamber formed therein. In one embodiment, for example, the electrodes are positioned between electrically insulative layers, and are positioned to directly contact a sample flowing through the microchannel formed therebetween (**FIG. 3D**).

[0062] The geometry, positioning, and/or arrangement of the electrodes is determined and/or selected to provide a constant value of ∇E_{rms}^2 sufficient for tracking particles within the isoDEP device. In one embodiment, selection and/or determination of the geometry, positioning, and/or arrangement of the electrodes is based, at least in part, upon the size and/or shape of the particles being tracked. For example, in **FIG. 3A**, Electrode 1 has a minimum radius of curvature of 50 μm while Electrode 2 is positioned such that a 10 V potential applied between the electrodes induces a value of ∇E_{rms}^2 sufficient to provide adequate passage of suspended particles and/or simultaneous observation of multiple cells having a diameter of between about 5 and 50 μm. Additionally or alternatively, applying a higher voltage facilitates the application of isoDEP to smaller cells. For example, a voltage amplifier may be used to apply voltages greater than 10 V, which facilitates tracking of smaller cells, widens the microchannel, and/or provides simultaneous viewing of more cells. In another example, decreasing the spacing between Electrode 1 and Electrode 2 increases the value of ∇E_{rms}^2 and facilitates application of isoDEP to smaller cells, such as, but not limited to, bacteria and/or mammalian cells having a diameter of between about 1 and 10 μm.

[0063] Turning to the microelectrode of **FIG. 3B**, in one embodiment, the extruded electrodes follow the curvature of the equipotential lines and/or form the wall of the microchannel itself. For a microelectrode isoDEP configuration (**FIG. 3B**), the relationship between k, the applied potential across the electrodes, ΔV, and the geometry of the device is

$$\Delta V = \frac{2}{3} k \left(\left(r_{60,2} \right)^{3/2} - \left(r_{60,1} \right)^{3/2} \right) \qquad (6)$$

where r_{60} refers to the distance between the origin and the respective equipotential line at $\theta = 60°$. Further, assuming small inner electrode curvature ($r_{60,1} \approx 0$) results in $k^2 = (9/4)\,\Delta V^2/(r_{60,2})^3$. Three-dimensional electrodes may be fabricated in a variety of ways, including sub-millimeter Computer Numeric Control (CNC) machining of a metal layer, electroplating, or deep reactive ion etching (DRIE) of highly-doped silicon wafers.

[0064] In some embodiments, as illustrated in **FIGS. 4A-E**, the microchannel defining electrodes of the system shown in **FIGS. 3A-E** are replaced with insulative features. The insulative features include similar or identical geometry, positioning, and/or arrangement as the microchannel defining electrodes described above. That is, geometrically, the same or similar boundary curvature is applied for both types of devices; with electrodes serving as sidewalls in **FIGS. 3A-E** and insulative material serving as sidewalls in **FIGS. 4A-E**. In embodiments where the insulative material serves as sidewalls, the electrodes are positioned upstream and downstream of the analytical space. These electrodes may include any suitable shape and/or size, including, but not limited to, shapes and sizes other than those described for the sidewall electrodes of the system shown in **FIGS. 3A-E**. As used herein, the term "upstream" refers to any location in a sample pathway before the analytical space, as determined with respect to a direction of flow through the device or system. The term "downstream," as used herein, refers to any location in a sample pathway after the analytical space, as determined with respect to a direction of flow through the device or system. In one embodiment, for example, the electrodes are positioned at a sample inlet and sample outlet of the system (**FIG. 4C**). In another embodiment, the upstream electrode is positioned anywhere between the sample inlet and the analytical space, and the downstream electrode is positioned anywhere between the analytical space and the sample outlet (**FIG. 4E**).

[0065] The equation of each line of voltage in the isoDEP field of the system including inlet and outlet electrodes is provided by replacing the sinusoidal term in Equation (4a) with a cosine term, giving Equation (4b). The resultant equipotential lines (solid lines) and electric field (dashed lines) are illustrated in **FIG. 4A**. An equipotential of $V = 0$ follows $\theta = 60°$ when potentials of opposite polarity are applied upstream and downstream from the origin. The resultant field will also produce a constant gradient of field squared, as in Equation (5).

[0066] As shown in **FIGS. 3B and 4A**, in contrast to the microchannel electrodes described above, which apply an electric field across the channel (**FIG. 3B**), the inlet and outlet electrodes apply an electric field through the channel (**FIG. 4A**). In some embodiments, a greater voltage is provided to apply the electric field through the channel as compared to the voltage provided to apply the electric flied across the channel. The resultant dielectrophoretic force is in the radial direction for both devices; particles will translate inward towards the origin for positive DEP and in the opposite direction for negative DEP.

[0067] Referring still to the insulative isoDEP shown in **FIG. 4A**, in one embodiment, the microchannel follows a similar curvature to that of the microelectrode design. In another embodiment, for the insulative isoDEP configuration of **FIG. 4A**, L is the distance from the origin to an upstream electrode. This results in $k_i^2 = (9/4)\,\Delta V^2/L^3$, which provides a difference in the applied potentials for each derived scenario (*e.g.*, $\Delta V = V$ applied across the r_{60} gap in **FIG. 3B** versus $\Delta V = 2V$ applied across $2L$ in **FIG. 4A**).

[0068] The use of insulative structures for dielectrophoresis has been extensively studied with most devices being fabricated out of glass or via soft lithography. Regardless of the fabrication method, in some embodiments, there are limitations in producing the precise inside corner at the $120°$ bend (dashed line, **FIG. 5**). Accordingly, in one embodiment, the insulative isoDEP system includes two curves that are more straightforward to fabricate. The variable r_{60} in **FIG. 5** refers to the distance between the origin and the respective curve at $\theta = 60°$. As such, the largest gap in the microchannel is $r_{60,2} - r_{60,1}$. The variable L refers to the distance between the origin and the electrode for insulative isoDEP devices (**FIG. 5**). **FIG. 5** also illustrates the resulting translation of a particle within an isoDEP environment. A particle experiencing nDEP will translate in the radial direction towards the origin; pDEP particles will translate radially in the opposite direction.

[0069] In some embodiments, a particle size (i.e., radius, a) is extracted through image analysis, leaving the Clausius-Mossotti factor (K_{CM}) as the only unknown parameter in Equation 1 above. In one embodiment, the particle reaches its terminal velocity within milliseconds of the application of field and the Clausius-Mossotti factor is extracted through DEP-induced particle velocimetry measurements (**FIGS. 6A-C**). Although shown with regard to a system including an electrode defined channel, as will be understood by those of ordinary skill in the art, a similar process including injecting a sample, applying a field, and acquiring an image may be used with a system including an insulative defined channel. In another embodiment, the particle's velocity changes as the AC frequency is swept over a specified range. In a further embodiment, the dielectric properties of the particle(s) are obtained by tracking each particle individually for a variety of applied AC field frequencies.

[0070] Accordingly, in one embodiment, the devices and/or methods described herein include determining and/or obtaining a detailed "particle velocity"/"frequency" spectrum for each tracked particle, which is similar to a "rotation speed"/"frequency" ROT spectrum (**FIG. 1**, right). That is, in some embodiments, the isoDEP device and/or method is and/or provides a translational equivalent to the rotational analysis of ROT. Thus, in another embodiment, the isoDEP device and/or method facilitates and/or provides simultaneous monitoring of the translation of many particles. In a further embodiment, this simultaneous monitoring improves DEP analytical throughput of individual particles and/or cells by at least one to two orders of magnitude, as compared to ROT.

[0071] The dielectric properties of the particle may be obtained by any suitable particle tracking method. For example, in one embodiment, tracking each particle individually includes single particle tracking velocimetry/spectroscopy. Particle tracking velocimetry is a technique to track a particle (typically in a liquid media) from acquired digital images. A microparticle typically reaches terminal velocity within a microfluidic environment within milliseconds. If an external (unknown) force is applied to a particle, hydrodynamic drag forces will counter it. Therefore, velocimetry measurement may be used to quantify an unknown external force. The radius of a particle needs to be determined, which can be estimated through various means including microscopic imaging. Additional optical characterization techniques (e.g., cell staining and fluorescent tagging) may be incorporated as well for comprehensive analysis. Furthermore, additional optical stimuli (e.g., optical tweezers, infrared photostimulation, etc.) may be incorporated to analyze the particle's response to external stimuli.

[0072] Unlike other DEP devices, isoDEP provides an electrokinetic analytical tool that is not meant to trap, divert, or concentrate particle samples. In some embodiments, electrokinetic techniques provide increased portability and/or decreased cost as compared to fluorescent techniques (e.g., flow cytometry). Accordingly, in one embodiment, the presently-disclosed subject matter may be applied to portable, remote diagnostic techniques, such as, for example, lab-on-chip technologies (e.g., first responders, remote environment monitoring, impoverished healthcare facilities). Additionally, as compared to existing DEP devices, advantages of the presently-disclosed subject matter include, but are not limited to, (i) providing a uniform DEP force that permits many particles to be observed simultaneously; (ii) providing application of straightforward microchannel injection without the need for precise particle placement relative to an electrode feature; (iii) permitting application of existing particle tracking velocimetry methods to extract K_{CM} information for each tracked cell simultaneously; and (iv) providing increased throughput.

[0073] In some embodiments, isoDEP provides high-throughput particle and/or cell analysis, including extraction of electrical and dielectric properties of each particle and/or cell (membrane permittivity/conductivity, cytoplasm permittivity/conductivity, etc.), which directly correlate to the cell physiology. Additionally or alternatively, the devices and/or methods described herein detect statistically significant variances in a particle sample (dielectric and/or geometry). In one embodiment, the devices and/or methods described herein provide analysis of cell subpopulations (i.e., individual analysis of cells). Analysis of cell subpopulations includes, but is not limited to, differentiation between different cell species, differentiation between physiological conditions (e.g., healthy and unhealthy), or a combination thereof. Suitable cell subpopulations include, but are not limited to, live and dead bacteria, healthy and damaged phytoplankton, breast cancer sublines, circulating tumor cells from non-transformed cells, leukocyte subpopulations (e.g., T lymphocytes, B lymphocytes, granulocytes, monocytes), and blood types. In another embodiment, isoDEP provides cell manipulation without or

substantially without damaging cells from exposure to the applied field. For example, the devices and/or methods may include the use of low-conductivity (e.g., < 1 S/m) media and/or effective heat transfer design to decrease or eliminate sample heating.

[0074] In certain embodiments, the devices and/or methods described herein include autonomous sample injection, image acquisition, and/or analyses. For example, in one embodiment, the devices and/or methods include isoDEP device integration, fluid handling (injection and valve control), visualization (camera optics, illumination, image acquisition), and/or data processing. In another embodiment, the devices and/or methods provide measurement of one hundred individual particles in less than ten minutes, which is an acquisition rate of approximately two orders of magnitude greater than ROT methods.

[0075] Also provided, in some embodiments of the presently-disclosed subject matter, are methods for individual particle analysis. In one embodiment, the method for individual particle analysis includes providing an isoDEP device, positioning a sample within the device, stopping or substantially stopping a flow of the sample within the device, applying an electric field to the device, and monitoring a translation of one or more particles in the samples. In another embodiment, applying the electric field to the device provides a constant value of ∇E_{rms}^2 in a viewing area thereof. In a further embodiments, the method includes determining one or more properties of the one or more particles based upon the translation of the particle(s). In some embodiments, the method facilitates and/or provides simultaneous monitoring of the translation of many particles.

[0076] Further provided herein, are methods of forming the isoDEP systems disclosed herein. In one embodiment, for example, a method of forming the isoDEP device illustrated in **FIGS. 3A-E** includes fabricating the electrodes through computer numeric controlled (CNC) machining (e.g., milling). The CNC machining includes any suitable sized and/or shaped bit to form the desired shape of the one or more electrodes. Suitable bits include, but are not limited to, bits having a diameter of 0.1 mm or smaller, such as, but not limited to, bits of between about 25 μm and 100 μm. In another embodiment, the curvature of the inner electrode boundary (Electrode 1, **FIG. 3A**) is limited by a diameter of the micrometer end-mill used during fabrication. In a further embodiment, for a minimum radius of curvature of 50 μm (i.e., using a 100 μm diameter bit), the resultant electrode perimeter is shown as "Electrode 1 boundary" in **FIG. 3A**.

[0077] In some embodiments, the size of the bits is selected such that the depth of the milled feature does not exceed twice the diameter of the bit. In some embodiments, the machining provides straight electrode sidewalls (< 5° taper) with a milled profile that matches the desired electrode boundary **(FIG. 3A)** to within 2 μm. Additionally or alternatively, in some embodiments, fabricating the electrodes includes forming one or more microfluidic channels therein. In some embodiments, the electrodes of the isoDEP device simultaneously serve as the microchannel walls. Accordingly, the electrodes may

include any material that is suitable for conducting electricity and/or compatible with the liquid sample. Suitable materials include, but are not limited to, copper, silver, gold, aluminum, doped silicon, or a combination thereof. As will be understood by those skilled in the art, the presently-disclosed subject matter is not limited to the examples described above and, in some embodiments, may include any other conductive material that is compatible with a liquid sample being used. The method may also include scaling an analytical solution to facilitate designing of the isoDEP device for a particular cell diameter.

[0078] In some embodiments, forming the isoDEP device includes electroplating the electrode material with one or more electroplating materials. Suitable electroplating materials include, but are not limited to, nickel, copper, chromium, zinc, tin, silver, gold, or a combination thereof. In one embodiment, the electroplating increases a biocompatibility of the electrodes and/or the isoDEP device. In another embodiment, after machining (e.g., milling) and/or electroplating the electrodes, the method includes sandwiching and/or at least partially surrounding the electrode with a substrate material. For example, in a further embodiment, the method includes spinning a thin film of UV epoxy onto two acrylic substrates, one of which includes fluid access ports, and sandwiching the machined material between the substrates. Next, the UV epoxy is cured and the substrate is diced into individual devices, isolating the two electrodes (**FIG. 7**). Conductive and non-conductive epoxy is then applied around a perimeter of the device to make electrical connections and seal the channels, respectively.

[0079] Although described above with regard to a milling procedure, as will be appreciated by those skilled in the art, any other suitable fabrication method may be used to form the isoDEP device described herein. For example, in an alternate embodiment, an additional high-precision micromilling machine with nanometer resolution and an assortment of 25 μm to 100 μm carbide square end mills is used. In another example, metallic laser cutting may be used. In a further example, highly-doped silicon wafers patterned via deep reactive ion etching (DRIE) is used; though etching is typically conducted in a clean room environment and is more costly.

[0080] In some embodiments, the isoDEP system including the insulative feature defined channel (**FIGS. 4A-E**) is formed from a mold. For example, in one embodiment, the mold is formed from Su-8, which is spun and pattered onto a base, such as a glass wafer. The Su-8 is pattered with any suitable geometry for the isoDEP platform, and includes a microchannel gap of any suitable size. After forming the geometry of the Su-8, inlet and outlet well features are connected with the microchannel to form the mold. In another embodiment, forming the isoDEP system includes pouring an insulative material over the mold and then curing the insulative material, such as, for example, by baking the material over the mold. Once cured, the insulative material is peeled from the mold and bonded to a planar insulative piece. The fluid inlets and outlets are then formed by any suitable method and the electrodes are provided therein. In certain embodiments, hollow needles are inserted into the cured material to form the fluid inlets and outlets and provide the electrodes in a single step.

[0081] Fabrication is not restricted to soft-lithography. There exists different insulative dielectrophoresis platforms that have been fabricated, typically, out of polymer (like PDMS) or glass. Insulative microfluidic devices can be fabricated via soft lithography, chemical etching, hot embossing, injection molding, CNC milling, or other established methods. Due to the similarity in fabrication methods, other insulative dielectrophoretic methods may incorporate isoDEP features in their system. One example is the incorporation of DC insulator DEP to introduce electrokinetic flow (combined electrophoresis and electro-osmosis). Also, contactless DEP (cDEP) may be used to prevent direct contact between the electrode and fluid sample.

[0082] In some embodiments, insulative dielectrophoretic systems decrease cost and/or reduce complexity of device fabrication as compared to those containing microelectrodes. In certain embodiments, the insulative isoDEP features are relatively large for microfluidic devices, including channel widths that are generally greater than 0.1 mm while still conforming to the curvature of the analytical solution (**FIG. 4A**). In addition, the preceding theoretical treatment of the insulative isoDEP system suggests that k_i may be, interestingly, independent of the microchannel gap (r_{60}) thus enabling flexibility in its design.

[0083] The presently-disclosed subject matter is further illustrated by the following specific but non-limiting examples. The following examples may include compilations of data that are representative of data gathered at various times during the course of development and experimentation related to the present invention.

EXAMPLES

[0084] <u>Example 1 – Calculation of a k_i value</u>

[0085] The following will calculate a value for k_i for a particular insulative isoDEP configuration. In this example, r_{60} refers to the distance between the origin and the respective insulator boundary at $\theta = 60°$ with the channel's largest gap being $r_{60,2}$-$r_{60,1}$. L is the distance from the origin to the electrode with an applied potential of V. Therefore, at $r = L$ and $\theta = 0°$,

$$V = \tfrac{2}{3} k_i L^{3/2} \quad \rightarrow \quad k_i^2 = \tfrac{9}{4} V^2 \left(\tfrac{1}{L^3} \right). \tag{7}$$

This analytical expression for k_i was used to compare experimental results with theory.

[0086] <u>Example 2 – Formation of a DEP system</u>

[0087] This Example describes formation of an analytical DEP system capable of measuring the dielectric properties of individual particles. The governing isoDEP equations were derived as disclosed above and applied to two different isoDEP prototypes: (i) one fabricated from deep reactive ion etching (DRIE) of a conductive silicon wafer (1-10 Ω-cm) whose patterned features served as electrodes and microchannel sidewalls simultaneously; (ii) a second where the electric field is applied lengthwise through a PDMS microchannel whose geometry follows a specific curvature.

[0088] Both positive and negative dielectrophoresis was demonstrated with the isoDEP devices using silver-coated hollow glass spheres and polystyrene particles, respectively. Particle tracking was used to compare particle trajectory with the expected dielectrophoretic response; further, particle velocity was used to measure the Clausius-Mossotti factor of individual polystyrene particles (18-24.9 μm) in both devices with a value of -0.40 ± 0.063 (n = 110) and -0.48 ± 0.055 (n = 18) for the DRIE and PDMS isoDEP platforms, respectively. The isoDEP platform is capable of analyzing multiple particles simultaneously, providing greater throughput than traditional electrorotation platforms.

[0089] <u>Example 3 – Determining length scale</u>

[0090] This example illustrates the required length scale of a microelectrode-based isoDEP device. In other words, determining a value of the gradient of the field-squared ($\|\nabla E_{rms}^2\| = k^2$) that would be sufficient for analyzing tracked particles within an isoDEP device. The translating particle has reached terminal velocity and its motion is balanced by the drag force ($\bar{F}_{DEP} = \bar{F}_{drag}$), resulting in a dielectrophoretic velocity (v_{DEP}) proportional to the dielectrophoretic force. Stokes' drag is assumed (neglecting wall influences) with a friction factor of $6\pi\mu a$ where μ is fluid viscosity. Variable values of the following exercise were arbitrarily chosen with fluid properties approximately those of water. For a particle radius of 5 μm, a $Re[f_{CM}]$ value of 0.1 (from a possible range of -0.5 to +1.0), a particle velocity of one particle diameter per second (10 μm/s), a fluid viscosity (μ) of 0.001 Pa-s, and a fluid relative permittivity of 80,

$$v_{DEP} = \frac{F_{DEP}}{6\pi\mu a} = \frac{2\pi\varepsilon_m a^3 Re[K_{CM}](\|\nabla E_{rms}^2\|)}{6\pi\mu a} \tag{8a}$$

$$\|\nabla E_{rms}^2\| = \frac{3\,v_{DEP}\,\mu}{a^2\,Re[K_{CM}]\,\varepsilon_m} = 1.7 \times 10^{13}\,\frac{V^2}{m^3}. \tag{8b}$$

[0091] Assume, for simplicity, that the inner electrode follows equipotential $V_1 = 0$ ($r_{60,1} = 0$). To meet the preceding parameters, with an applied potential of V_2 = 100 V the electrode will have a width of $r_{60,2}$ = 1.10 mm; this value reduces to 0.24 mm for V_2 = 10 V. This example illustrates how the governing analytical expressions can be used to design and scale an appropriate isoDEP platform based on the experimental parameters (ex: rate or image acquisition, voltage limits, etc.). The analytical solution provides a design parameter such that the electrode geometry can be properly configured and adapted for a variety of cell sizes.

[0092] It is noted that Equation (1) assumes a stationary field. However, if there is a spatial non-uniformity in the electric field's phase (φ), the extended DEP force is given by

$$F_{DEP} = 2\pi\varepsilon_s a^3 Re[K_{CM}]\nabla E_{rms}^2 + 4\pi\varepsilon_s a^3 Im[K_{CM}]\left(E_{rms,x}^2\nabla\varphi_x + E_{rms,y}^2\nabla\varphi_y + E_{rms,z}^2\nabla\varphi_z\right) \tag{9}$$

The second term is dependent on the imaginary part of the Clausius-Mossotti factor and the spatial non-uniformity of the field's phase. In particular, a rotating field will induce particle rotation, a phenomenon called electrorotation (ROT).

[0093] It is significant to note the similarity between isoDEP and electrorotation (ROT) for the electrokinetic analysis of single particles. ROT is a technique that involves the use of rotating fields generated, typically, by a four-electrode rotating-field system and has been used to differentiate cells. The rotational speed of the particle is measured as a function of the applied frequency and subsequent particle dielectric properties are determined from correlating these measurements to the imaginary component of the Clausius-Mossotti factor. For this isoDEP platform a particle's velocity will change as the AC frequency is swept over a specified range in accordance to a varying a $Re[K_{CM}]$. As such, isoDEP is essentially the translational equivalent of the rotational analysis in ROT. The primary disadvantages of ROT are the requirement of a rotating field and its limited throughput. The described isoDEP technique, however, requires a common AC potential and can track multiple particles that are simultaneously exposed to the same gradient of field-squared.

[0094] *Examples 4-10 are directed to the isoDEP system including the electrode defined channel.*

[0095] Example 4 - Comparison with Other Techniques.

[0096] A general overview comparing flow cytometry, EIS (static and dynamic), ROT, and isoDEP is shown in Table 1. isoDEP provides a detailed, sensitive measurement for each cell which is as sensitive as ROT and static EIS. Additionally, although the processing rate of isoDEP is may be less than that of flow cytometry and dynamic EIS, it is at least one to two orders of magnitude greater than ROT and static EIS. Furthermore, in certain embodiments, the cost of isoDEP device fabrication and operation is significantly lower than the other techniques.

[0097] First, isoDEP devices can be fabricated using a benchtop micromill as opposed to cleanroom fabrication methods (unlike ROT, EIS microfluidic chips) which comparatively require significant infrastructure and facilities. Second, isoDEP operation requires a benchtop waveform generator and a digital camera which is a significant reduction in operation cost compared to ROT (four-channel waveform generators), static EIS (impedance analyzers), and, especially, flow cytometry. Reduced costs also enable more frequent tests which is important for applications that require frequent monitoring. Another advantage is the portability of isoDEP.

	Label-Free	Cell Throughput (per second)	Sensitive Measurements	Fabrication and Operation Expense
Flow Cytometry		1000s	✓	$ $
Electrorotation	✓	< 1	✓	$
EIS: Dynamic	✓	1000s		$
EIS: Static	✓	< 1	✓	$ $
isoDEP	✓	10s-100s	✓	0-$

[0098] **Table 1.** General overview comparing various cell subpopulation analytical techniques. $: Requires specialized fabrication facilities (i.e. cleanroom) or specialized equipment for operation. $$: Requires specialized fabrication facilities and specialized equipment for operation.

[0099] Example 5 – Analysis of phytoplankton.

[00100] Phytoplankton growth is a function of light and temperature, buoyancy, inorganic nutrient availability, interactions with organic compounds, organic micronutrients, and competition and predation factors. Phytoplankton assemblages in water bodies have been studied extensively over the past century and are excellent indicators of environmental conditions that determine water quality. Therefore, understanding the physiological status of live phytoplankton cells in aquatic environments (e.g., the detection of healthy or unhealthy phytoplanktonic cells) is important because of their function as primary producers, their position at the base of aquatic food webs, and their ability to rapidly respond to environmental change. A recent, significant example of this came about on August 2, 2014 when environmental monitors for Toledo determined that microcysin toxin in public water supplies had levels higher than recommended by the World Health Organization. Residents could not drink or cook with tap water and boiling water would not be effective.

[00101] Several DEP methods have been used on phytoplankton cells that identify, sort, and electrokinetically characterize their viability of freshwater. *Neochloris oleoabundans* has been sorted and concentrated for biofuel production using DEP. Electrorotation has been used to distinguish between viable-healthy and non-viable *Tetraselmis* cells in marine environments. Insulator-based DEP has been used to examine the dielectric properties of the cell membranes of viable and non-viable *Selenastrum capricornutum*, a common freshwater species. The development of isoDEP methods described herein would (1) decrease the cost of electrokinetic characterization of cells as compared to other methods, and (2) provide portability in the field (onto water bodies) for real-time analysis of the physiological status of phytoplankton assemblages *in situ*. This information would give important insight into the overall health of an aquatic ecosystem.

[00102] Several taxa of phytoplankton may be used to test the isoDEP concept (**Table 2**). These taxa are not intended to limit the application of the presently-disclosed subject matter, rather, they are

selected because they (1) are significant representatives of phytoplanktonic assemblages in freshwater ecosystems, (2) are geographically ubiquitous and, therefore, lend comparative power to other studies, (3) are variable in size and shape, (4) are indicators of a wide range of environmental conditions ("algal blooms"), (5) are physiologically diverse and comparable (e.g., one *Microcystis* strain is capable of producing microcystin, a noxious toxin in freshwaters, while another *Microsystis* strain does not), (6) are relatively easy to culture and maintain, (7) are easily induced into log-phase growth ("healthy" cells) prior to experimentation, (8) are commercially available, and (9) can be transported easily.

TABLE 2

Taxon	Division	Cell Shape	Cell Size	Commercial Source
Chlorella vulgarus	Chlorophyta	Spheroid	10 μm	Carolina
Selenastrum capricornutum	Chlorophyta	Crescent	10 μm	UTEX
Cyclotella meneghiniana	Bacillariophyta	Discoid	15–30 μm	UTEX
Cymbella tumida	Bacillariophyta	Crescent	50 μm	UTEX
Microcystis aeringinosa (non-toxic, non-microcystin producing)	Cyanophyta	Spheroid	5–7 μm	UTEX
Microcystis aeringinosa (microcystin producing)	Cyanophyta	Spheroid	5–7 μm	UTEX

[00103]   The tested species include two species of green algae, *Chlorella vulgaris* and *Selenastrum capricornutum* (Chlorophyceae), two diatoms, *Cyclotella meneghiniana* and *Cymbella tumida* (Bacillariophyceae), and two strains of blue-green bacteria, *Microcystis aeringinosa* (Cyanophyceae). Toxin-producing and non-toxin producing strains of *Microcystis* lend another ecophysiological dimension to comparisons in that *Microcystis* is a significant problem in highly productive (eutrophic) systems. *Microcystis* toxin (microtoxin) causes severe and acute toxicological responses in other aquatic organisms when subjected to bloom conditions. All identified species are ubiquitous in freshwater phytoplanktonic assemblages and are relatively easy to culture and maintain.

[00104]   Phytoplankton cultures used in this project are maintained under sterile conditions in Percival incubators at Hancock Biological Station (HBS), Murray State University (Murray, KY). Maintenance of actively metabolizing and growing phytoplankton cultures takes place in accordance with methods of Lorenz et al. The physiological status of cultures is monitored and cells will be prepared for experimentation using methods of MacIntyre and Cullen. Appropriate QA/QC procedures are adhered to for cultures over the course of this study. Comparisons of the physiological response of healthy cells by isoDEP are made with cells that are senescing (out of log-phase growth) or killed (by boiling or poisoning).

[00105]   By measuring the electrokinetic response of several freshwater phytoplankton species (**Table 2**), isoDEP provides identification and differentiation thereof. Rapid, accurate detection of potentially harmful algal blooms and degraded water quality using isoDEP methods indicates a positive

outcome from these experiments that will contribute to other applications in unhealthy or otherwise compromised aquatic systems (e.g., polluted, contaminated, eutrophic). An advantage of using isoDEP technology in water quality studies is that it is rapid, accurate, and can detect subtle changes in algal cell health (and, thus, ecosystem health), and can be taken into the field (on shipboard) for instant results without having to collect, maintain, and transport live samples back to a land-based laboratory for testing.

[00106]   Example 6 – Fabrication and system operation.

[00107]   A commercially available miniature end mill (Mini-Mill 1, Minitech Machinery, Norcross, GA), which has a spindle accuracy of 0.8 μm and spindle speed up to 60,000 rpm, is used for this example. A 100 μm end mill is used to create the electrodes from copper sheets as outlined in **FIG. 7**. The milled features include the electrode geometry as well as microfluidic channels (**FIG. 7A**). After machining the specified features in the copper sheet, the metal is electroplated with nickel then gold to provide a robust finish to their product. Further, the plated layer of gold aids in electrode biocompatibility.

[00108]   Next, a thin film of UV epoxy is spun onto two acrylic substrates (one of which contains fluid access ports) that are used to sandwich the machined metal sheet. After curing, the substrate is diced into individual devices (**FIG. 7B**) which subsequently isolates the two electrodes (**FIG. 7C**). Finally, conductive and non-conductive epoxy is applied around the perimeter of the device to make electrical connections and seal the channels, respectively (**FIG. 7C**).

[00109]   Using the process above, a milled DEP quadropole device was formed using a copperclad PCB substrate. The quadropole electrode from this work is shown in **FIG. 8**, and was created using a 100 μm bit with the copperclad substrate and subsequent DEP trapping of 8 μm particles. This demonstrated that straight-sidewall 3D electrodes can be milled from a 36 μm thick copper layer, thereby making the electrodes of the device serve simultaneously as the microchannel walls (similar in principle to the proposed isoDEP device).

[00110]   Example 7 – Confirmation of isomotive DEP field.

[00111]   To confirm that the isoDEP device design exerts a constant DEP force on similar particles, identical homogeneous spherical polystyrene microparticles (size-standard 10 μm) will be injected into the isoDEP device and, upon electric field activation, all particles should translate at the same constant velocity regardless of their position within the channel. The device will be mounted on an inverted microscope (Nikon Ti-U) and particles will be visualized using a 4X objective and digital camera (PCO Sensicam QE). Images will be acquired such that individual particle velocity can be extracted. Free PTV software (accumulated and posted on his research website) will be utilized for velocimetry analysis.

[00112]   The goal will be to observe constant particle velocity over the acquired field-of-view. Characteristics that would inhibit this goal would be derived from the fabrication of the device itself. A particle velocimetry map of the microchannel will be obtained to determine if identified velocimetry inconsistencies are specific to a particular microchannel region or feature. Alternatively, velocimetry inconsistencies may be attributed to the statistically inhomogeneous distribution of particle diameters (results will be compared accordingly).

[00113]   Fluorescent imaging will be used for more precise particle tracking (i.e. tracking the individual particle's fluorescent peak). However, fluorescent analysis is nontrivial to implement for portable micro-devices and alternative methods may need to be sought for future development. For example, particle shadow velocimetry (PSV) uses a pulsed LED and has demonstrated velocimetry resolution comparable to fluorescent/excited PIV methods. Proper cell imaging cannot be overlooked since morphological information for each particle can be extracted accordingly and, further, the cell's size gives insight into its DEP force (which is directly proportional to the volume of the particle).

[00114]   <u>Example 8 – Demonstrate bead subpopulation identification.</u>

[00115]   In this example a heterogeneous sample containing multiple particle diameters and types is tested. Larger particles of the same type are expected to experience faster DEP-induced velocities as the DEP force scales with particle volume (Equation 1); therefore, particles of different diameter may be identified using isoDEP. Further, particles of different type (polystyrene, silica) experience different $Re[f_{CM}]$ values at different AC frequencies and, therefore, may be differentiated with the isoDEP device. Polystyrene and silica, in particular, have similarly-shaped $Re[f_{CM}]$ profiles but have measureable differences in their crossover frequency (i.e. the frequency at which $Re[f_{CM}] = 0$); isoDEP is able to resolve the different particle types accordingly.

[00116]   For some known particle diameter (a), particle velocity (v_{DEP}), and field gradient (∇E_{rms}^2), the Clausius-Mossotti factor may be extracted from isoDEP measurements. As such, frequency-dependent $Re[f_{CM}]$ measurements of polystyrene and silica particles are compared to those in literature (these particle types are found extensively in DEP experimental research) and evaluated for similarity.

[00117]   <u>Example 9 – Assess unwanted electrokinetic effects in isoDEP devices.</u>

[00118]   There were several aforementioned electrokinetic effects that may interfere with particle translation within an isoDEP device, namely ACEO, ET flow, and Joule heating. This example provides electrokinetic observations for a range of DEP-relevant frequencies (1 kHz – 10 MHz), voltages (< 20 V), and medium conductivities (10 mS/m – 1 S/m). Although described with a frequency range of from 1 kHz to 10 MHz, other frequency ranges may be used, including, but not limited to, 100 Hz - 100 MHz, 1 kHz – 100 MHz, 1 MHz – 100 MHz, 10 MHz – 100 MHz, or any suitable combination, sub-combination, range, or sub-range thereof. First, numerical simulations are conducted to predict expected

electrohydrodynamic behavior. Second, 2 μm fluorescent polystyrene particles is injected and tracked under various AC field and fluid conductivities in order to assess the significance of the other electrokinetic effects. To assess Joule heating, the chip is monitored by an in-house infrared microscope (InfraScope, OFI Corporation) to directly measure field-induced heating.

[00119]   Based upon the measurements above, the appropriate range of operation parameters for the isoDEP device to minimize unwanted electrokinetic effects is determined. However, it is expected that electrohydrodynamic mechanisms (ACEO, ET flow) will be *significantly* reduced compared to traditional coplanar electrode designs (ex: interdigitated electrodes); coplanar electrodes are characterized by regions of extremely high localized fields (i.e. at electrode edges) which is not an inherent characteristic of isoDEP electrodes.

[00120]   <u>Example 10 – Design and fabrication.</u>

[00121]   A proof-of-concept design was fabricated at the University of Louisville Micro/Nano Technology Center. The electrodes for the final device were constructed from a highly doped silicon wafer (0.35 mm thick, B-doped to a resistivity of 1-10 Ω-cm).

[00122]   *Selection of Electrode Geometry.* In theory, any two arbitrary equipotential lines can be chosen as long as they are of the form (using polar coordinates)

$$V = \frac{2}{3}kr^{3/2}sin\left(\frac{3\theta}{2}\right) \qquad\qquad (4a)$$

The equipotential lines, and thus the electrode geometry, were initially chosen as follows:

[00123]   The inner Electrode 1 is assigned a curvature with a minimum radius of 0.5 mm. Even though an inner electrode with a perfect 120° is acceptable, there are inherent challenges associated with fabricating a 'perfect' inner corner without some degree of curvature. The minimum distance that the Electrode 1 equipotential curve will be from the origin will occur at $\theta = 60°$ calculated with

$$r_{1,min} = \frac{r}{cos30} - r = 77.35\ \mu m \qquad\qquad (P1)$$

[00124]   Assumptions are needed to determine a value of k. Assuming Stoke's drag on a spherical particle that has reached terminal velocity, its DEP-induced velocity is

$$v_{DEP} = \frac{2\pi\varepsilon_m a^3 Re[f_{CM}]\nabla E_{rms}^2}{6\pi\ a\ \mu} \quad\rightarrow\quad \nabla E_{rms}^2 = k^2 = \frac{3\ v_{DEP}\ \mu}{a^2\ Re[f_{CM}]\ \varepsilon_m} \qquad (P2)$$

Assuming a particle radius, a, of 10 μm, viscosity of 0.001 Pa-s, a $Re[f_{CM}]$ value of 0.1, medium relative permittivity of 80, and a velocity of one diameter per second, the resultant values are

$$\nabla E_{rms}^2 = k^2 = 8.471e12, \quad k = 2.91e6 \qquad\qquad (P3)$$

[00125]   For a known r_{min} (from P1), $\theta = 60°$, and k (from P3) the value of V_1 for the Electrode 1 is 1.320 V. The curvature of Electrode 1 is (for this example)

$$V_1 = 1.320 = \frac{2}{3}(2910454.9)r^{3/2}sin\left(\frac{3\theta}{2}\right) \tag{P4}$$

[00126]   The curvature of Electrode 2 is determined through an assumed applied voltage. For an assumed voltage difference of 100 V, the curvature of Electrode 2 is

$$V_2 = (100 + 1.320) = \frac{2}{3}(2910454.9)r^{3/2}sin\left(\frac{3\theta}{2}\right) \tag{P5}$$

[00127]   Two device sizes were used for proof-of-concept demonstration. Each design used the same inner Electrode 1 profile. A second device assumed a voltage difference of 50 V, leading to a curvature of

$$V_3 = (50 + 1.320) = \frac{2}{3}(2910454.9)r^{3/2}sin\left(\frac{3\theta}{2}\right) \tag{P6}$$

[00128]   In summary, the curvatures chosen for one of the devices is V_1 and V_2 and those of the second device is V_1 and V_3. Any electrode profiles can be chosen following this method.

[00129]   The variable r_{60} is used here to describe the largest gap distance between the two electrodes for a particular device, this occurs at a value of $\theta = 60°$. The larger device ($\Delta V = 100$ V) has a value of $r_{60,1} = 1319.7$ μm whereas the smaller device ($\Delta V = 50$ V) has a value of $r_{60,2} = 810.4$ μm.

[00130]   A photolithographic mask was created using these features with the design shown in **FIG. 9**.

[00131]   *Fabrication.* For fabrication, the 4" silicon doped wafer was anodically bonded to a 4" diameter borosilicate glass wafer (0.7 mm thick) followed by DRIE of the pattern. Next, a second glass wafer was anodically bonded on the other side of the silicon wafer. Finally, the wafer was diced to produce the final devices. The diced wafer is shown in **FIG. 10A** and an individual device is shown in **FIG. 10B** with two identical channels.

[00132]   *Preliminary Tests with Beads.* The following describes preliminary testing of the above isomotive DEP proof-of-concept device using microparticles suspended in liquid media. According to theory, a particle will translate towards or away from the device's origin (**FIG. 5**) depending on if the particle is experiencing negative DEP or positive DEP, respectively.

[00133]   The devices were tested using polystyrene particles (24.9 μm diameter, carboxylate modified, Spherotech) and silver coated hollow glass spheres (5-30 μm diameter, Cospheric). The particles were suspended in a deionized water solution with an electrical conductivity less than 1 mS/m. Electrical wires were affixed to the electrodes at the perimeter of the device using conductive epoxy. The sample was injected manually with a syringe and was adjusted until bulk fluid motion halted. An AC signal was then applied across the channel (1 kHz to 10 MHz, up to 100 V_{rms}). The device was viewed with an inverted microscope (Nikon Ti) using a 2X objective lens.

[00134]   **FIG. 11A** shows a composite image of polystyrene particles traveling towards the origin exhibiting negative DEP (nDEP) for an AC signal of 100 kHz and 34.4 V. The shown overlaid particle

images represent their respective position after several 1.25 second intervals. Preliminary qualitative observations suggest that the velocity of each particle is nearly constant (i.e. their spacing between each time step is consistent) and, further, particles translate in a radial direction; a more detailed particle tracking analysis is ongoing.

[00135]   FIG. 11B shows a composite image of silver coated particles translating away from the origin exhibiting positive DEP (pDEP) for an AC signal of 500 kHz at 33 V. The shown overlaid particle images represent their respective position after 0.67 second intervals. Consistent with the negative DEP results, translation is away from the origin of the device at a consistent rate. Consistent with DEP theory, larger particles translate at a greater velocity.

[00136]   FIGS. 12A-B show the path and linear fit for 110 individual particles undergoing nDEP as in FIG. 11A. FIGS. 13A-B show scaled particle velocity and deviation of particle trajectory from the theoretical direction, respectively.

[00137]   It is important to note that even though this was demonstrated with a microfabricated device with DRIE there are many alternatives to device fabrication. As long as the channel/electrode walls are electrically conductive and vertical (depth-wise) the device should perform as above. In some embodiments, non-vertical walls or walls containing "rough" features will generate edge effects that will compromise particle translation for those in close proximity to the wall; this can be eliminated with proper fabrication. Further, if the particles are focused to the channel center (e.g., hydrodynamic stream) these unwanted effects can be further minimized.

[00138]   *Examples 11-12 are directed to isoDEP systems including the insulative feature defined channel.*

[00139]   Example 11 – Design and fabrication.

[00140]   For proof-of-concept demonstration of insulative isoDEP a PDMS microfluidic device was fabricated from a master mold of Su-8, a common procedure for microfluidic devices. In brief, a single layer of Su-8 50, approximately 100 μm thick, was spun and pattered onto a soda-lime glass wafer. The patterned mimicked the geometry of the previous microelectrode isoDEP platform with a microchannel gap of 500 μm at $\theta = 60°$ ($r_{60,1} = 77$ μm, $r_{60,2} = 577$ μm). Inlet and outlet well features of 2.0 mm diameter were connected with the microchannel; their center was approximately 3.0 mm from the device origin. An illustration of the Su-8 mold geometry is shown in FIG. 4B. PDMS was poured over the master mold and baked in an oven at 65 °C for at least two hours. After curing, the PDMS was peeled from the mold and plasma bonded to a planar PDMS piece. Fluid inlets and outlets were created by inserting 22 gauge stainless steel needles; the needles themselves also simultaneously served as device electrodes (FIG. 4B). The AC signal originated at an arbitrary waveform generator (Keithley 3390) and was amplified using an in-house custom-built amplifier; the output signal was monitored using a benchtop oscilloscope.

[00141]   Example 12 – Testing Dielectrophoretic Behavior

[00142]   Two types of particles were used to test the dielectrophoretic behavior of the insulative isoDEP device. Carboxylate modified polystyrene particles, 18-24.9 μm in diameter (Spherotech, Inc.), and silver-coated hollow glass particles, 5-30 μm in diameter (Cospheric LLC), where used to demonstrate negative DEP and positive DEP, respectively. Particles were suspended in low conductivity water (0.2-0.5 mS/m) before being injected manually into the device via a syringe. The center of the device was observed ("Observation area", **FIG. 4B**) with an inverted microscope (Nikon Ti-U) with 3X magnification and videos were recorded with a color camera (DCC1645C-HQ, ThorLabs) at 15 frames per second. Bulk flow was manually adjusted until flow was observed to be stagnant with one or more particles in the observation area. Particles settled to the bottom of the microchannel before the AC field was applied. The applied AC signal for all reported experiments was 300 V at 2 kHz; for this system's L of approximately 3 mm the resulting applied field is on the order of 50 V/mm.

[00143]   Multiple videos of polystyrene particles were acquired and analyzed similarly as previously demonstrated. In brief, videos were color inverted and converted to grayscale before being process with TrackMate, an ImageJ plugin that measures particle position and their respective diameter. A custom MATLAB program used the measured position data to calculate particle velocity and trajectory. All particle tracking data was cropped to 60 frames (2.0 seconds). For proper comparison between similar particles, a scaled dielectrophoretic velocity (v_{DEP}/a^2) was calculated for each one. Next, scaled velocity was used to determine each particle's Clausius-Mossotti factor ($Re[f_{CM}]$). Last, the trajectory of each particle was fit to a linear path and used to calculate, to what extent, it deviated from the theoretical radial translation.

[00144]   **FIGS. 14A-B** demonstrates the trajectory of translating particles undergoing negative DEP (**FIG. 14A**) and positive DEP (**FIG. 14B**) at 300 V and 2 kHz using an insulating isoDEP device with a r_{60} gap of 500 μm. The particles translated in the radial direction in accordance with expected theory. Particle spacing between overlaid images (2.0 seconds apart for **FIG. 14A**, 0.33 seconds for **FIG. 14B**) is consistent, suggesting relatively constant dielectrophoresis-induced velocity. Further, the insert in **FIG. 14B** shows the chaining of two particles aligned in the direction of the applied field; interestingly, inherent to the nature of this insulative isoDEP system, the direction of the dielectrophoretic force is approximately orthogonal to the direction of the electric field near $\theta = 60°$, and transitions to the radial direction near 0° and 120°. Since the direction of the dielectrophoretic force is known and constant for this isoDEP device, the influence DEP force and directionality on particle-chain formation and integrity could be extensively studied.

[00145]   The trajectories of 18 polystyrene particles subjected to negative dielectrophoresis are shown in **FIG. 15**. Compared to previous results using the microelectrode isoDEP device (**FIG. 3B**), the

trajectories of the insulative isoDEP device were not significantly influenced when the particles were in close proximity to the wall, this was likely due to the smooth contour of the microchannel. In some cases bulk fluid motion was observed and, to some extent, compromised the trajectory of the particles; future versions of the isoDEP system will incorporate to eliminate bulk fluid motion during electrokinetic analysis.

[00146]   Another factor that influences particle translation is the influence of the microchannel wall on the exerted hydrodynamic drag which is a function of the particle's proximity to a planar surface. A particle in close proximity to a surface can experience over three times greater hydrodynamic drag and, even though sufficient time was allowed to have the tracked particles sediment prior to field activation, their depth-wise position may not be consistent. In addition, the nature of Su-8 photolithography produces sidewalls that are slightly inclined, though that did not appear to significantly influence results; however, deep-reactive ion etching could be used to create a master mold with vertical walls, as demonstrated previously with other electrokinetic microfluidic chips, and may be considered for future insulative isoDEP devices.

[00147]   For the particles studied undergoing negative DEP, their scaled velocities (v_{DEP}/a^2) were measured and 12/18 were within 10% of the mean and 17/18 were within 20%. The trajectory of every tracked particle was within 20° of the theoretical radial trajectory with 15/18 being within 10°. Next, a particle's scaled velocity was used to determine their respective Clausius-Mossotti factor using

$$v_{DEP} = \frac{2\pi\varepsilon_m a^3 Re[f_{CM}]\nabla E_{rms}^2}{C_w\, 6\pi\, a\, \mu} \quad\rightarrow\quad Re[f_{CM}] = \left(\frac{v_{DEP}}{a^2}\right)\left(\frac{3\mu C_w}{\varepsilon_m k_i^2}\right) \qquad (10)$$

where C_w is the hydrodynamic drag correction due to the influence of the wall (assumed to be 3.08) and μ is fluid viscosity (assumed to be 0.00089 Pa-s); the relative permittivity of the fluid was assumed to be 80. The gradient field squared (k_i^2) was calculated to be 3.36×10^{11} V^2/m^3 using Eqn. (7) with $V = 150$ V and $L = 2.48$ mm (electrode distance was measured visually using feedback from the microscope's motorized stage). The average $Re[f_{CM}]$ for the tracked 18 particles was -0.48 with a standard deviation of 0.055. This result is in close proximity to the theoretical value of -0.50 and, further, demonstrated closer convergence to the theoretical value compared the first microelectrode isoDEP study that had a value of -0.40 for the same particles.

[00148]   Unlike microelectrode based isoDEP devices where the electrodes themselves may serve as heat sinks (FIG. 3B), insulative isoDEP devices (FIG. 4A) are primarily constructed from the same material (PDMS for this work). Since the thickness of the device is much smaller than its footprint (millimeters compared to centimeters), conductive heat transfer through its thin boundaries will be the primary mode of heat transfer. Therefore, significant temperature gradients will be generated orthogonal to the direction of the electric field, a desirable system characteristic in order to reduce the effects of electrothermal flow. As such, similar to the previous isoDEP device, electrothermal hydrodynamic

motion was observed under certain experimental conditions. Using low-conductivity media (0.2-0.5 mS/m) no significant electrothermal flow was observed at the upper limit of the amplifier (~400 V). Using diluted PBS (35 mS/m), electrothermal motion was observed starting at approximately 300 V. Future work will model various insulative isoDEP designs to determine how to significantly reduce electrothermal flow, especially for higher conductivity biological media.

[00149]   *Examples 13-18 are directed to isoDEP systems including both the electrode based and insulative feature defined channel.*

[00150]   Example 13 – Design and fabrication of the electrode based isoDEP device.

[00151]   Two fabrications procedures were implemented to demonstrate proof-of-concept isoDEP using both methodologies. For the microelectrode version, several devices were created with r_{60} electrode gaps ranging from 0.25 mm to 1.4 mm. Fabrication followed a procedure where a highly doped silicon wafer (0.35 mm thick, 1-10 Ω-cm) was patterned via deep reactive ion etching (DRIE) and anodically bonded between two borosilicate glass wafers. The decision to fabricate devices via DRIE was made due to the straight vertical features associated with this microfabrication procedure; tapered electrode sidewalls would generate inconsistent fields and would distort the goal of attaining a constant gradient field-squared. That is, the straight sidewalls provided a constant depth-wise application of the field.

[00152]   **FIG. 3E** shows a completed microelectrode isoDEP device with $r_{60,1}$ = 77 μm and $r_{60,2}$ = 577 μm (i.e. a 500 μm r_{60} gap). The device was mounted to a microscope slide with quick-drying epoxy; the epoxy was also used to seal the "Electrode Gaps" (**FIG. 3E**) that prevented electrical shorting between the adjacent electrodes. A diamond bur (0.9 mm diameter, 801L/009C, Crosstech) was subsequently used to drill holes into the upper glass substrate and enable fluid access. Next, pieces of single-sided rubber adhesive (FDA-compliant silicone rubber, #8991K52, McMaster-Carr) with punched holes served as ports to interface the device with plastic tubing. Electrical connections to the device were accomplished by applying conductive epoxy (CW2400, Circuit Works) to the perimeter of the device at the exposed portions of the doped silicon electrodes; thin wires were embedded in the conductive epoxy and cured in a 60 °C oven for 20 minutes.

[00153]   Example 14 - Design and fabrication of the insulator-based isoDEP device

[00154]   For the insulative isoDEP platform (**FIG. 4B**), a PDMS microfluidic device was fabricated via soft lithography from a master mold of Su-8, a common procedure for microfluidic devices. In brief, a single layer of Su-8 50, approximately 120 μm thick, was spun and pattered onto a soda-lime glass wafer. The microchannel was designed with a gap of 500 μm at θ = 60° ($r_{60,1}$ = 77 μm, $r_{60,2}$ = 577 μm). The centers of the inlet and outlet wells (2 mm in diameter) were 3.0 mm from the device origin. PDMS was poured over the master mold and baked in an oven at 65 °C for at least two hours. After curing, the PDMS was peeled from the mold and plasma bonded to a planar PDMS piece.

Fluid inlets and outlets were created by inserting 22 gauge stainless steel needles; the needles themselves also simultaneously served as device electrodes (**FIG. 4B**).

[00155]   Example 15 – Experimental methods

[00156]   The AC signal originated at an arbitrary waveform generator (Keithley 3390) and subsequently amplified using either a commercial benchtop amplifier (2100HF, Trek; up to 150 V, 1 MHz) or an in-house custom-built amplifier (up to ~800 V, 10 kHz). The signal output was monitored with a benchtop digital multi-meter (Agilent 34405A).

[00157]   For qualitative experiments carboxylate modified polystyrene particles, 18-24.9 μm in diameter (Spherotech, Inc.), and silver-coated hollow glass particles, 5-30 μm in diameter (Cospheric LLC), were used to demonstrate nDEP and pDEP, respectively. Particles were suspended in low conductivity water (0.6 mS/m) before being injected manually into the device. A portion of the sample was viewed at the device's center ("Observation area", **FIGS. 3E and 4C**) using an inverted microscope (Nikon Ti-U) with trans-illumination, digital images were acquired with a color camera (DCC1645C-HQ, ThorLabs). Flow was manually adjusted until one or more particles were observed in the viewing area, at that time a quarter-turn flow valve was closed to halt flow. Particles were allowed to sediment (< 1 min.) before the AC field was applied. For quantitative nDEP experiments, a video was acquired at 15 fps for at least 10 seconds after the application of the field. This process was repeated until the trajectories of a number of polystyrene particles were recorded ($n = 110$ for microelectrode isoDEP, $n = 18$ for insulative isoDEP). Grayscale and color inversion filters were applied with video-editing software (VirtualDub) before being processed with ImageJ. TrackMate, a particle tracking plug-in for ImageJ (imagej.net/TrackMate), was used to measure particle diameter and position for each video frame. Particles that were adhered to a surface or collided with an electrode wall were omitted from particle tracking analysis.

[00158]   A custom MATLAB program determined particle velocity and trajectory from particle position data. First, all particle tracking data was cropped to a common length (165 frames or 11 seconds for microelectrode isoDEP, 60 frames or 4.0 seconds for insulative isoDEP). Next, for each respective particle identified within a particular frame, i, its initial position within that frame was extracted (x_i, y_i) as well as its coordinates for the next four subsequent frames (x_{i+1}, y_{i+1}; x_{i+2}, y_{i+2}; x_{i+3}, y_{i+3}; x_{i+4}, y_{i+4}). A straight line was fit to these points to determine its mean displacement in the x- and y-directions over these five frames; mean velocity was subsequently calculated from the mean displacement divided by the time period of five frames. Next, the calculated particle velocities from each frame were averaged over the duration of its trajectory for an overall average particle velocity. A scaled velocity (v_{DEP}/a^2) was also calculated for each particle using their respective measured particle diameter ($2a$); in theory, the scaled velocity for like particles should be identical for isoDEP if all other experimental conductions are held constant. Further, the Clausius-Mossotti factor ($Re[K_{CM}]$) was

calculated from the measured scaled velocity with additional assumptions regarding the properties of the fluid. Last, each particle's trajectory was fit to a linear path; the angle at which this fitted path deviated from the theoretical radial trajectory (**FIG. 5**) is termed a particle's "angle of deviation".

[00159]   For the microelectrode isoDEP device, qualitative pDEP and nDEP experiments were conducted with a 800 μm device ($r_{60,1}$ = 77 μm, $r_{60,2}$ = 877 μm) at frequencies of 500 kHz and 100 kHz, respectively, with an applied potential of 34 V. The applied voltage and curvature, using the preceding analysis, results in k^2 = 1.5 × 10^{13} V^2/m^3. Quantitative microelectrode isoDEP tests were conducted with a 500 μm device ($r_{60,1}$ = 77 μm, $r_{60,2}$ = 577 μm) at 100 kHz and 15 V (k^2 = 2.91×10^{12} V^2/m^3). For the insulative isoDEP device, the applied AC signal was 300 V at 2 kHz; this results in k_i^2 = 3.36×10^{11} V^2/m^3 using with V = 150 V and L = 2.48 mm (electrode distance was measured visually using feedback from the microscope's motorized stage). The applied frequencies for these cases were arbitrarily chosen as the observed velocities of the particles did not change over a range of tested frequencies (1 kHz – 1 MHz, data not shown); this was expected as the Clausius-Mossotti factor would be relatively independent of AC frequency for large (> 2 μm) homogeneous particles.

[00160]   Example 16 – Demonstration of nDEP and pDEP

[00161]   **FIGS. 11A-B** and **14A-B** illustrate nDEP of polystyrene particles and pDEP of silver-coated hollow glass particles using both isoDEP devices. Following expected theory, the particles translated in the radial direction, either towards (nDEP) or away (pDEP) from the origin. Further, qualitatively, particle translation appears to be constant during its trajectory as demonstrated with consistent spacing between particle images. Refer to Supporting Information for experimental videos demonstrating isoDEP particle translation using negative and positive DEP.

[00162]   Electro-orientation of adhered particles is highlighted for the pDEP cases (**FIGS. 11B, 14B**); their alignment is consistent with the direction of the electric field. Interestingly, inherent to the nature of the insulative isoDEP system, the direction of the dielectrophoretic force is approximately orthogonal to the direction of the electric field near θ = 60°, and transitions to the radial direction near 0° and 120°. Since the direction of the dielectrophoretic force is known (and constant) for isoDEP, the influence that the DEP force and directionality on particle-chain formation and integrity could be studied.

[00163]   Example 17 – Particle trajectory

[00164]   Next, polystyrene particles were tracked for quantitative evaluation of the devices' performance. Particle trajectories (**FIGS. 12A** and **15**) were consistently migrating towards the device origin. However, in specific regions within the channel the particle motion deviates from theory, particularly for the microelectrode device when colloids are in close proximity to the wall of the microchannel. DRIE inherently does not produce smooth features; as such, rough electrode features will distort the electric field in close proximity to the wall and, therefore, compromise particle trajectory,

detracting it from the theorized motion. Relatively, the trajectories of the insulative isoDEP device were not significantly influenced when the particles were in close proximity to the wall; this was likely due to the smoother contour of the PDMS microchannel. In addition, the nature of Su-8 photolithography produces sidewalls that are slightly tapered, though that did not appear to significantly influence results; however, DRIE could be used to create a master mold with vertical walls, as demonstrated previously with other electrokinetic microfluidic chips, and may be considered for future insulative isoDEP devices.

[00165] In addition, slight (though significant) bulk fluid motion was observed due to the use of flexible tubing and use of valves relatively far from the device's ports. The impact of bulk fluid motion is illustrated in the "jagged" trajectories of some of the particles (**FIG. 12A**). Future isoDEP platforms will incorporate rigid tubing and proper valving to reduce bulk fluid motion. For subsequent analysis, a linear fit was applied to the trajectory of each respective particle (refer to Supporting Information).

[00166] Next, for each particle, their respective scaled velocity (v_{DEP}/a^2) was normalized with their average. In theory, for similar homogeneous particles their behavior should be identical (i.e. a value of 1.0). In general, particles close to the center of the device performed more consistently compared to those further from the perimeter. For the microelectrode isoDEP device 55/110 and 91/110 of the particles were within 10% and 20% of the average scaled velocity, respectively. For the insulative isoDEP device 12/18 were within 10% of the mean and 17/18 were within 20%. Bulk fluid motion was likely the source of the observed systematic error (refer to Supporting Information).

[00167] The angle of deviation from a particle's linear trajectory to that of the theoretical radial direction was determined (i.e. a value of $0°$ means particle trajectory follows theory). For the microelectrode isoDEP device, 77/110 and 107/110 of the particles were within $10°$ and $20°$ of the theoretical trajectory, respectively (refer to Supporting Information). Every tracked particle was within $20°$ of the theoretical radial trajectory for the insulative isoDEP device with 15/18 being within $10°$.

[00168] Velocity data was used to extract the Clausius-Mossotti factor for each particle using Eqn. 7a and making assumptions on fluid properties (a viscosity of 0.000890 Pa-s and a relative permittivity of 80). Further, it was assumed that the particle translated adjacent to the bottom of the microchannel as the electric field was applied once the particles settled; this characteristic increases the hydrodynamic drag by an assumed factor of 3.08 (Faxén's correction [40]), a reasonable approximation compared to previous works [41, 42]. The average $Re[K_{CM}]$ for the population of studied particles for the microelectrode and insulative isoDEP devices were -0.40 ±0.063 (one standard deviation) and -0.48 ± 0.055. Theoretically this value should be -0.50 for $\sigma_p \ll \sigma_m$; more precise knowledge of fluid properties, particle location with respect to the microchannel wall, and dielectric composition of the particle would improve the accuracy of the acquired experimental values of $Re[f_{CM}]$ herein.

[00169] Example 18 – Observed electrohydrodynamics

[00170]   Electrohydrodynamic motion was observed at larger applied potentials (> 50V for microelectrode isoDEP, > 400 V for insulator isoDEP); a more comprehensive investigation will be conducted in future work to determine the impact of such fluid motion on particle trajectory. Electrohydrodynamic motion, in general, is either AC electro-osmosis (ACEO) and/or electrothermal (ET) flow. ACEO occurs when the electric field acts upon the charges accumulated on the surface of a polarized electrode, inducing hydrodynamic slip. It is expected that this isoDEP device will produce negligible ACEO flow as the tangential component of the electric field at the electrode surface is significantly weaker compared to other studied ACEO microelectrode geometries like interdigitated electrodes. Therefore, it is hypothesized that ET flow is the cause of the observed electrohydrodynamic motion. In ET flow the electric field acts upon dielectric gradients (permittivity, conductivity) in the fluid caused by Joule heating. The silicon in the microelectrode isoDEP device may serve as a heat sink as well as provide more efficient heat transfer (compared to the glass boundaries) and, thus, propagate temperature gradients in the same direction as the applied field. Insulative isoDEP systems are likely more favorable from a heat transfer perspective as temperature gradients are more orthogonal to the field direction relative to the silicon-based devices, thereby reducing the effects of electrothermal flow. Future work will study the heat transfer and resulting electrohydrodynamics of isoDEP devices.

[00171]   *Results of Examples 13-18*

[00172]   *Device Considerations.* The allure of insulative dielectrophoretic systems is the inexpensive cost and reduced complexity of device fabrication compared to those containing microelectrodes, though a significantly higher voltage is required for similar DEP performance. Regardless of the fabrication method chosen, isoDEP features are relatively large when compared to traditional microfluidic devices as microchannel widths are generally greater than 0.1 mm; however, conforming to the curvature of the analytical solution (**FIGS. 3B** and **4A**) is important for proper device performance. Particular to insulative isoDEP devices k_i may be, interestingly, independent of the microchannel gap (for $L \gg r_{60}$), thus enabling flexibility in its design.

[00173]   Due to the similarity in fabrication methods, other insulative dielectrophoretic methods may integrate isoDEP into their system. One example is the integration of DC insulator-based DEP to introduce electrokinetic flow (combined electrophoresis and electro-osmosis). Also, contactless DEP may be used to prevent direct contact between the electrode and fluid sample. The suppression of unwanted flow (bulk flow, electrohydrodynamics) coupled with ideal electrode fabrication (smooth parallel sidewalls) will result in unhindered particle trajectory.

[00174]   *Concluding remarks.* The dielectrophoresis systems introduced here produced a uniform gradient of the field-squared ($\|\nabla E_{rms}^2\|$), providing a constant, isomotive dielectrophoretic force throughout the region of observation. This was demonstrated using microelectrodes and an insulative microchannel both following a specific curvature. Experiments demonstrated both positive and negative

dielectrophoresis; the Clausius-Mossotti factor can be measured for individual particles using particle tracking velocimetry. It is worth reiterating that such particle-tracking analysis is non-trivial for DEP systems where the dielectrophoretic force is not constant and the location of the particle (relative to the electrode) needs to be determined. The purpose of the isoDEP platform is to extract the complex frequency-dependent Clausius-Mossotti factor of individual particles, similar in concept to electrorotation. However, in traditional electrorotation the particle needs to experience nDEP simultaneously for analysis whereas isoDEP can analyze particles undergoing pDEP and nDEP. Further, a significantly higher throughput of isoDEP is expected over traditional electrorotation platforms, including at least one to two orders of magnitude greater throughput. Moreover, this platform provides optical access to the sample enabling the integration of optically-based manipulation (ex: optical tweezers) and analysis (ex: immunostaining) enabling comprehensive single-cell analysis.

[00175]   Example 19 – Derivation of Equations (4a) and (4b)

[00176]   The potential. V, in a charge-free region of space between two electrodes is described by the Laplace equation:

$$\nabla^2 V = 0 \qquad\qquad (D1)$$

With the constraint set that the resulting dielectrophoretic force is applied in the radial direction only, the solution of the Laplacian in cylindrical coordinates is

$$V = Ar^n \sin(n\theta) \qquad\qquad (D2)$$

where A and n are constants. For $\bar{E} = -\nabla V$ the equation is:

$$\bar{E} = -\left(\frac{\partial V}{\partial r}\right)\hat{r} - \left(\frac{1}{r}\right)\left(\frac{\partial V}{\partial \theta}\right)\hat{\theta} \qquad\qquad (D3)$$

$$\bar{E} = -nAr^{n-1}\left(\sin(n\theta)\,\hat{r} + \cos(n\theta)\,\hat{\theta}\right) \qquad\qquad (D4)$$

$$E^2 = \bar{E} \cdot \bar{E} = n^2 A^2 r^{2n-2} \qquad\qquad (D5)$$

$$\nabla(E^2) = 2(n-1)n^2 A^2 r^{2n-3}\hat{r} \qquad\qquad (D6)$$

[00177]   In order for the resulting dielectrophoretic force to be constant it requires that $2n - 3 = 0$ or $n = 3/2$ such that:

$$\nabla(E^2) = \left(\frac{3A}{2}\right)^2 \hat{r} \qquad\qquad (D7)$$

A substitution of another constant $k = 3A/2$ yields Equation 4a

$$V = \frac{2}{3} k\, r^{3/2} \sin(3\theta/2) \qquad\qquad (4a)$$

[00178]   The above derivation for a constant gradient field squared is valid for Equation (4b) as well

$$V = \frac{2}{3} k_i\, r^{3/2} \cos(3\theta/2) \qquad\qquad (4b)$$

[00179]   All publications, patents, and patent applications mentioned in this specification are herein incorporated by reference to the same extent as if each individual publication, patent, or patent application was specifically and individually indicated to be incorporated by reference, including the references set forth in the following list:

REFERENCES

1.   Morgan, H. and Green, N.G., *AC Electrokinetics: Colloids and Nanoparticles*. 2003, Philadelphia, PA: Research Studies Press.

2.   Pethig, R., *Review article-dielectrophoresis: status of the theory, technology, and applications*. Biomicrofluidics, 2010. **4**(2).

3.   Wood, N.R., Wolsiefer, A.I., Cohn, R.W., and Williams, S.J., *Dielectrophoretic trapping of nanoparticles with an electrokinetic nanoprobe*. Electrophoresis, 2013. **34**(13): p. 1922-30.

4.   Williams, S.J., Romero, N., Parkes, L., Jackson, D.J., and Naber, J.F., *Inexpensive three-dimensional dielectrophoretic microfluidic devices using milled copperclad substrates*. Journal of Electrostatics, 2015. **75**: p. 49-53.

5.   Khoshmanesh, K., Nahavandi, S., Baratchi, S., Mitchell, A., and Kalantar-zadeh, K., *Dielectrophoretic platforms for bio-microfluidic systems*. Biosensors & Bioelectronics, 2011. **26**: p. 1800-1814.

6.   Li, H.B., Zheng, Y.N., Akin, D., and Bashir, R., *Characterization and modeling of a microfluidic dielectrophoresis filter for biological species*. Journal of Microelectromechanical Systems, 2005. **14**(1): p. 103-112.

7.   Bunthawin, S., Ritchie, R.J., and Wanichapichart, P., *Dielectrophoresis of Tetraselmis sp., a unicellular green alga, in travelling electric field analyzed using the RC model for a spheroid*. Songklanakarin Journal of Science and Technology, 2011. **33**(5): p. 585-597.

8.   Cristofanilli, M., De Gasperis, G., Zhang, L., Hung, M.C., Gascoyne, P.R., and Hortobagyi, G.N., *Automated electrorotation to reveal dielectric variations related to HER-2/neu overexpression in MCF-7 sublines*. Clin Cancer Res, 2002. **8**(2): p. 615-9.

9.   Sano, M.B., Henslee, E.A., Schmelz, E., and Davalos, R.V., *Contactless dielectrophoretic spectroscopy: examination of the dielectric properties of cells found in blood*. Electrophoresis, 2011. **32**(22): p. 3164-71.

10.   Han, S.I., Joo, Y.D., and Han, K.H., *An electrorotation technique for measuring the dielectric properties of cells with simultaneous use of negative quadrupolar dielectrophoresis and electrorotation*. Analyst, 2013. **138**(5): p. 1529-37.

11.   Srivastava, S.K., Daggolu, P.R., Burgess, S.C., and Minerick, A.R., *Dielectrophoretic characterization of erythrocytes: positive ABO blood types.* Electrophoresis, 2008. **29**(24): p. 5033-46.

12.   Wang, X.J., Yang, J., and Gascoyne, P.R.C., *Role of peroxide in AC electrical field exposure effects on Friend murine erythroleukemia cells during dielectrophoretic manipulations.* Biochimica Et Biophysica Acta-General Subjects, 1999. **1426**(1): p. 53-68.

13.   Archer, S., Li, T.T., Evans, A.T., Britland, S.T., and Morgan, H., *Cell reactions to dielectrophoretic manipulation.* Biochemical and Biophysical Research Communications, 1999. **257**(3): p. 687-698.

14.   Jones, T.B., *Electromechanics of Particles.* 1995, Cambridge ; New York: Cambridge University Press.

15.   Gimsa, J., *A comprehensive approach to electro-orientation, electrodeformation, dielectrophoresis, and electrorotation of ellipsoidal particles and biological cells.* Bioelectrochemistry, 2001. **54**(1): p. 23-31.

16.   Chang, H.C. and Yeo, L.Y., *Electrokinetically driven microfluidics and nanofluidics.* 2010, Cambridge ; New York: Cambridge University Press. xvi, 508 p., 8 p. of plates.

17.   Ramos, A., *Electrokinetics and electrohydrodynamics in microsystems.* CISM courses and lectures. 2011, Wien ; New York: Springer. 297 p.

18.   Ajdari, A., *Pumping liquids using asymmetric electrode arrays.* Physical Review E, 2000. **61**(1): p. R45-R48.

19.   Ramos, A., Morgan, H., Green, N.G., and Castellanos, A., *AC electrokinetics: a review of forces in microelectrode structures.* Journal of Physics D-Applied Physics, 1998. **31**(18): p. 2338-2353.

20.   Bazant, M.Z. and Squires, T.M., *Induced-charge electrokinetic phenomena.* Current Opinion in Colloid & Interface Science, 2010. **15**(3): p. 203-213.

21.   Levitan, J.A., Devasenathipathy, S., Studer, V., Ben, Y., Thorsen, T., Squires, T.M., and Bazant, M.Z., *Experimental observation of induced-charge electro-osmosis around a metal wire in a microchannel.* Colloids and Surfaces A: Physiochem. Eng. Aspects, 2005. **267**: p. 122-132.

22.   Bazant, M.Z. and Squires, T.M., *Induced-charge electrokinetic phenomena: theory and microfluidic applications.* Phys Rev Lett, 2004. **92**(6): p. 066101.

23.   Gonzalez, A., Ramos, A., Green, N.G., Castellanos, A., and Morgan, H., *Fluid flow induced by nonuniform ac electric fields in electrolytes on microelectrodes. II. A linear double-layer analysis.* Physical Review E, 2000. **61**(4): p. 4019-4028.

24.   Green, N.G., Ramos, A., Gonzalez, A., Morgan, H., and Castellanos, A., *Fluid flow induced by nonuniform ac electric fields in electrolytes on microelectrodes. I. Experimental measurements.* Physical Review E, 2000. **61**(4): p. 4011-4018.

25.   Green, N.G., Ramos, A., Gonzalez, A., Morgan, H., and Castellanos, A., *Fluid flow induced by nonuniform ac electric fields in electrolytes on microelectrodes. III. Observation of streamlines and numerical simulation.* Physical Review E, 2002. **66**(2).

26.   Olesen, L.H., Bruus, H., and Ajdari, A., *AC electrokinetic micropumps: The effect of geometrical confinement, Faradaic current injection, and nonlinear surface capacitance.* Physical Review E, 2006. **73**: p. 056313.

27.   Ramos, A., Gonzalez, A., Castellanos, A., Green, N.G., and Morgan, H., *Pumping of liquids with AC voltages applied to asymmetric pairs of microelectrodes.* Physical Review E, 2003. **67**: p. 056302.

28.   Ramos, A., Morgan, H., Green, N.G., and Castellanos, A., *AC electric-field-induced fluid flow in microelectrodes.* Journal of Colloid and Interface Science, 1999. **217**(2): p. 420-422.

29.   Castellanos, A., Ramos, A., Gonzalez, A., Green, N.G., and Morgan, H., *Electrohydrodynamics and dielectrophoresis in microsystems: scaling laws.* Journal of Physics D-Applied Physics, 2003. **36**(20): p. 2584-2597.

30.   Green, N.G., Ramos, A., Gonzalez, A., Castellanos, A., and Morgan, H., *Electrothermally induced fluid flow on microelectrodes.* Journal of Electrostatics, 2001. **53**(2): p. 71-87.

31.   Green, N.G., Ramos, A., Gonzalez, A., Castellanos, A., and Morgan, H., *Electric field induced fluid flow on microelectrodes: the effect of illumination.* Journal of Physics D-Applied Physics, 2000. **33**(2): p. L13-L17.

32.   Mizuno, A., Nishioka, M., Ohno, Y., and Dascalescu, L.D., *Liquid Microvortex Generated around a Laser Focal Point in an Intense High-Frequency Electric-Field.* IEEE Transactions on Industry Applications, 1995. **31**(3): p. 464-468.

33.   Nakano, M., Katsura, S., Touchard, G.G., Takashima, K., and Mizuno, A., *Development of an optoelectrostatic micropump using a focused laser beam in a high-frequency electric field.* IEEE Transactions on Industry Applications, 2007. **43**(1): p. 232-237.

34.   Williams, S.J., *Enhanced electrothermal pumping with thin film resistive heaters.* Electrophoresis, 2013. **34**: p. 1400-1408.

35.   Antar, B.N. and Nuotia-Antar, V.S., *Fundamentals of Low Gravity Fluid Dynamics and Heat Transfer.* 1993, Boca Raton, FL: CRC Press.

36.   Puttaswamy, S.V., Sivashankar, S., Chen, R.J., Chin, C.K., Chang, H.Y., and Liu, C.H., *Enhanced cell viability and cell adhesion using low conductivity medium for negative dielectrophoretic cell patterning.* Biotechnol J, 2010. **5**(10): p. 1005-15.

37.   Banada, P.P., Liu, Y.S., Yang, L., Bashir, R., and Bhunia, A.K., *Performance evaluation of a low conductive growth medium (LCGM) for growth of healthy and stressed Listeria monocytogenes and other common bacterial species.* Int J Food Microbiol, 2006. **111**(1): p. 12-20.

38.   Pethig, R., *Dielectrophoresis: Status of the theory, technology, and applications.* Biomicrofluidics, 2010. **4**: p. 022811.

39.   Sun, T., Morgan, H., and Green, N.G., *Analytical solutions of ac electrokinetics in interdigitated electrode arrays: electric field, dielectrophoretic and traveling-wave dielectrophoretic forces.* Phys Rev E Stat Nonlin Soft Matter Phys, 2007. **76**(4 Pt 2): p. 046610.

40.   Muller, T., Gradl, G., Howitz, S., Shirley, S., Schnelle, T., and Fuhr, G., *A 3-D microelectrode system for handling and caging single cells and particles.* Biosensors & Bioelectronics, 1999. **14**(3): p. 247-256.

41.   Schnelle, T., Muller, T., Gradl, G., Shirley, S.G., and Fuhr, G., *Paired microelectrode system: dielectrophoretic particle sorting and force calibration.* Journal of Electrostatics, 1999. **47**(3): p. 121-132.

42.   Martinez-Duarte, R., *Microfabrication technologies in dielectrophoresis applications - A review.* Electrophoresis, 2012. **33**: p. 3110-3132.

43.   Voldman, J., Gray, M.L., Toner, M., and Schmidt, M.A., *A microfabrication-based dynamic array cytometer.* Analytical Chemistry, 2002. **74**(16): p. 3984-3990.

44.   Srivastava, S.K., Gencoglu, A., and Minerick, A.R., *DC insulator dielectrophoretic applications in microdevice technology: a review.* Analytical and Bioanalytical Chemistry, 2011. **399**(1): p. 301-321.

45.   Salmanzadeh, A., Kittur, H., Sano, M.B., C Roberts, P., Schmelz, E.M., and Davalos, R.V., *Dielectrophoretic differentiation of mouse ovarian surface epithelial cells, macrophages, and fibroblasts using contactless dielectrophoresis.* Biomicrofluidics, 2012. **6**(2): p. 24104-2410413.

46.   Sano, M.B., Caldwell, J.L., and Davalos, R.V., *Modeling and development of a low frequency contactless dielectrophoresis (cDEP) platform to sort cancer cells from dilute whole blood samples.* Biosensors & Bioelectronics, 2011. **30**(1): p. 13-20.

47.   Sano, M.B., Salmanzadeh, A., and Davalos, R.V., *Multilayer contactless dielectrophoresis: Theoretical considerations.* Electrophoresis, 2012. **33**(13): p. 1938-1946.

48.   Shafiee, H., Caldwell, J.L., Sano, M.B., and Davalos, R.V., *Contactless dielectrophoresis: a new technique for cell manipulation.* Biomedical Microdevices, 2009. **11**(5): p. 997-1006.

49.   Gencoglu, A., Camacho-Alanis, F., Nguyen, V.T., Nakano, A., Ros, A., and Minerick, A.R., *Quantification of pH gradients and implications in insulator-based dielectrophoresis of biomolecules.* Electrophoresis, 2011. **32**(18): p. 2436-2447.

50.   Yang, J., Huang, Y., Wang, X.B., Becker, F.F., and Gascoyne, P.R., *Differential analysis of human leukocytes by dielectrophoretic field-flow-fractionation.* Biophys J, 2000. **78**(5): p. 2680-9.

51.   Engel, J., Donath, E., and Gimsa, J., *Electrorotation of Red-Cells after Electroporation.* Studia Biophysica, 1988. **125**(1): p. 53-62.

52.   Kalodimou, V.E. and AABB., *Basic principles in flow cytometry.* 2013, Bethesda, Md: AABB Press. xiv, 91 p.

53.   Malleo, D., Nevill, J.T., Lee, L.P., and Morgan, H., *Continuous differential impedance spectroscopy of single cells.* Microfluid Nanofluidics, 2010. **9**(2-3): p. 191-198.

54.   Cheung, K., Gawad, S., and Renaud, P., *Impedance spectroscopy flow cytometry: on-chip label-free cell differentiation.* Cytometry A, 2005. **65**(2): p. 124-32.

55.   Gawad, S., Holmes, D., Benazzi, G., Renaud, P., and Morgan, H., *Impedance spectroscopy and optical analysis of single biological cells and organisms in microsystems.* Methods Mol Biol, 2010. **583**: p. 149-82.

56.   Wetzel, R.G., *Limnology : lake and river ecosystems.* 3rd ed. 2001, San Diego: Academic Press. xvi, 1006 p.

57.   Schor, A.R. and Buie, C.R. *Non-invasive sorting of lipid producing microalgae with dielectrophoresis using microelectrodes.* in *ASME 2012 International Mechanical Engineering Congress and Exposition.* 2012. Houston, TX.

58.   Wanichapichart, P., Wongluksanapan, T., and Khooburat, L. *Electrorotation: Diagnostic tool for abnormality of marine phytoplankton cells.* in *Proceedings of the 2nd IEEE International Conference on Nano/Micro Engineered and Molecular Systems.* 2007. Bangkok, Thailand.

59.   Gallo-Villanueva, R.C., Jesus-Perez, N.M., Martinez-Lopez, J.I., Pacheco, A., and Lapizco-Encinas, B.H., *Assessment of microalgae viability employing insulator-based dielectrophoresis.* Microfluidics and Nanofluidics, 2011. **10**: p. 1305-1315.

60.   Stephenson, R.J. and Smol, J.P., *Use of algae in environmental assessments,* in *Freshwater Algae of North America: Ecology and Classification,* J.D. Wehr and R.G. Sheath, Editors. 2003, Academic Press: New York. p. 775-804.

61.   Lembi, C.A., *Control of nuisance algae*, in *Freshwater Algae of North America: Ecology and Classification*, J.D. Wehr and R.G. Sheath, Editors. 2003, Academic Press: New York. p. 805-834.

62.   Shubert, E., *Nonmotile coccoid and colonial green algae*, in *Freshwater Algaue of North America: Ecology and Classification*, J.D. Wehr and R.G. Sheath, Editors. 2003, Academic Press: New York. p. 253-310.

63.   Pohl, H.A., *Dielectrophoresis: The Behavior of Neutral Matter in Nonuniform Electric Fields.* 1978, Cambridge; New York: Cambridge University Press.

64.   Cambron, S.D., Franco-Sarabia, J.R., Walsh, K.M., and Keynton, R.S. *Micromachined tacks for retinal implant applications.* in *3rd Annual International IEEE EMBS Spectial Topic Conference on Microtechnologies in Medicine and Biology.* 2005. Kahuku, Oahu, Hawaii.

65.   Hu, N., Yang, J., Yin, Z.Q., Ai, Y., Qian, S., Svir, I.B., Xia, B., Yan, J.W., Hou, W.S., and Zheng, X.L., *A high-throughput dielectrophoresis-based cell electrofusion microfluidic device.* Electrophoresis, 2011. **32**(18): p. 2488-95.

66.   Graham, D.M., Messerli, M.A., and Pethig, R., *Spatial manipulation of cells and organelles using single electrode dielectrophoresis.* Biotechniques, 2012. **52**(1): p. 39-43.

67.   Li, S., Yuan, Q., Morshed, B.I., Ke, C., Wu, J., and Jiang, H., *Dielectrophoretic responses of DNA and fluorophore in physiological solution by impedimetric characterization.* Biosens Bioelectron, 2013. **41**: p. 649-55.

68.   Iliescu, C., Xu, G.L., Ong, P.L., and Leck, K.J., *Dielectrophoretic separation of biological samples in a 3D filtering chip.* Journal of Micromechanics and Microengineering, 2007. **17**(7): p. S128-S136.

69.   Iliescu, C., Xu, G.L., Samper, V., and Tay, F.E.H., *Fabrication of a dielectrophoretic chip with 3D silicon electrodes.* Journal of Micromechanics and Microengineering, 2005. **15**(3): p. 494-500.

70.   Williams, S.J., Park, C., and Wereley, S.T., *Recent advances and applications of micro-PIV.* Microfluidics and Nanofluidics, 2010. **8**(6): p. 709-726.

71.   Khodaparast, S., Borhani, N., Tagliabue, G., and Thome, J.R., *A micro particle shadow velocimetry (μPSV) technique to measure flows in microchannels.* Experiments in Fluids, 2013. **54**: p. 1474.

72.   Wei, M.T., Junio, J., and Ou-Yang, H.D., *Direct measurements of the frequency-dependent dielectrophoresis force.* Biomicrofluidics, 2009. **3**(1).

73.   Lorenz, M., Friedl, T., and Day, J.G., *Perpetual maintenance of actively metabolizing microalgal cultures*, in *Algal Culturing Techniques*, R.A. Anderson, Editor. 2005, Elsevier Academic Press: New York. p. 145-163.

74.   MacIntyre, H.L. and Cullen, J.J., *Using cultures to investigate the physiological ecology of microalgae*, in *Algal Culturing Techniques*, R.A. Anderson, Editor. 2005, Elsevier Academic Press: New York. p. 287-326.

75.   Andersen, R.A., *Algal culturing techniques.* 2005, Burlington, Mass.: Elsevier/Academic Press. x, 578 p.

76.   Williams, S.J., Kumar, A., Green, N.G., and Wereley, S.T., *Optically induced electrokinetic concentration and separation of colloids.* Journal of Micromechanics and Microengineering, 2010. **20**.

77.   Kumar, A., Kwon, J.-S., Williams, S.J., Green, N.G., Yip, N.K., and Wereley, S.T., *Optically modulated electrokinetic manipulation and concentration of colloidal particles near an electrode surface.* Langmuir, 2010. **26**(7): p. 5262-5272.

78.   Kumar, A., Williams, S.J., Chuang, H.S., Green, N.G., and Wereley, S.T., *Hybrid opto-electric manipulation in microfluidics - opportunities and challenges.* Lab on a Chip, 2011. **11**: p. 2135-2148.

79.   Sifferlin, A., *Toledo's contaminated water: here's what went wrong*, in *Time*. 2014.

80.   Drees, J., *Signature Partnership celebrates five years of community service*, in *The Louisville Defender*. 2012: Louisville, Kentucky.

81.   Xia, Y. and G.M. Whitesides, *Soft Lithography.* Angew Chem Int Ed Engl, 1998. **37**: p. 550-575.

82.   Jaqaman, K., et al., *Robust single-particle tracking in live-cell time-lapse sequences.* Nat Methods, 2008. **5**(8): p. 695-702.

83.   Karanfilian, S.K. and T.J. Kotas, *Drag on a sphere in unsteady motion in a liquid at rest.* Journal of Fluid Mechanics, 1978. **87**: p. 85-96.

84.   Zellner, P., et al., *Off-chip passivated-electrode, insulator-based dielectrophoresis (OpiDEP).* Anal Bioanal Chem, 2013. **405**(21): p. 6657-66.

85.   Elvington, E.S., et al., *Label-free isolation and enrichment of cells through contactless dielectrophoresis.* J Vis Exp, 2013(79).

86.   Kim, S. and S.J. Karrila, *Microhydrodynamics : principles and selected applications.* 2005, Mineola, N.Y.: Dover Publications. xxiii, 507 p.

87.   Gonzalez, A., et al., *Electrothermal flows generated by alternating and rotating electric fields in microsystems.* Journal of Fluid Mechanics, 2006. **564**: p. 415-433.

88.   Barrett, L.M., et al., *Dielectrophoretic manipulation of particles and cells using insulating ridges in faceted prism microchannels.* Anal Chem, 2005. **77**(21): p. 6798-804.

89.   Hawkins, B.G., et al., *Continuous-flow particle separation by 3D Insulative dielectrophoresis using coherently shaped, dc-biased, ac electric fields.* Anal Chem, 2007. **79**(19): p. 7291-300.

90.   Srivastava, S.K., A. Gencoglu, and A.R. Minerick, *DC insulator dielectrophoretic applications in microdevice technology: a review.* Anal Bioanal Chem, 2011. **399**(1): p. 301-21.

91.   Shafiee, H., et al., *Contactless dielectrophoresis: a new technique for cell manipulation.* Biomed Microdevices, 2009. **11**(5): p. 997-1006.

[00180]   It will be understood that various details of the presently disclosed subject matter can be changed without departing from the scope of the subject matter disclosed herein. Furthermore, the foregoing description is for the purpose of illustration only, and not for the purpose of limitation.

CLAIMS

What is claimed is:

1.   A method of analyzing particles, comprising:
        providing an isomotive dielectrophoresis device;
        positioning a sample within the device, the sample including at least one particle;
        applying an electric field to the device, the electric field inducing a constant
dielectrophoresis force on the at least one particle of the sample; and
        monitoring a translation of the at least one particle.

2.   The method of claim 1, wherein the at least one particle includes a cell.

3.   The method of claim 1, wherein positioning the sample within the device comprises
injecting the sample into the device until bulk fluid motion is halted.

4.   The method of claim 1, wherein the constant dielectrophoresis force comprises a
constant force within an analytical space of the device.

5.   The method of claim 1, wherein applying the electric field to the device comprises
applying an AC signal across a channel in the device.

6.   The method of claim 5, wherein the AC signal is between 100 Hz and 100 MHz.

7.   The method of claim 1, wherein applying the electric field to the device comprises
applying an AC signal through a channel in the device.

8.   The method of claim 1, further comprising extracting dielectric properties of the at
least one particle.

9.   The method of claim 8, further comprising determining a cell physiology from the
dielectric properties.

10.   An isomotive dielectrophoresis device, comprising:

a first electrode having a first surface geometry;

a second electrode having a second surface geometry; and

an electrically insulating material at least partially surrounding the first electrode and the second electrode;

wherein the first electrode and the second electrode are arranged and disposed to provide a constant dielectrophoresis force within an analytical space of the device.

11.   The device of claim 10, wherein the first electrode and the second electrode are arranged and disposed to provide a constant gradient field-squared within the analytical space of the device.

12.   The device of claim 10, wherein the first electrode and the second electrode define a microchannel therebetween.

13.   The device of claim 12, wherein the constant dielectrophoresis force is applied across the microchannel.

14.   The device of claim 12, wherein the analytical space of the device comprises a portion of the microchannel.

15.   A method of forming the device of claim 10, the method comprising:

selecting a curvature of the first electrode and a curvature of the second electrode based upon the equation $V = \frac{2}{3} kr^{3/2} sin\left(^{3\theta}/_2\right)$.

16.   An isomotive dielectrophoresis device, comprising:

a first insulative feature having a first surface geometry;

a second insulative feature having a second surface geometry; and

at least one electrode positioned upstream and at least one electrode positioned downstream of an analytical space;

wherein the first insulative feature and the second insulative feature are arranged and disposed to form a microchannel extending from the inlet to the outlet of the device; and

wherein the first surface geometry of the first insulative feature and second surface geometry of the second insulative feature are arranged and disposed to provide a constant dielectrophoresis force within an analytical space of the device.

17.   The device of claim 16, wherein the first electrode and the second electrode are arranged and disposed to provide a constant electrical field gradient within the analytical space of the device.

18.   The device of claim 16, wherein the constant dielectrophoresis force is applied through the microchannel.

19.   The device of claim 16, wherein the analytical space of the device comprises a portion of the microchannel.

20.   A method of forming the device of claim 16, the method comprising:

        selecting a curvature of the first electrode and a curvature of the second electrode based upon the equation $V = \frac{2}{3}kr^{3/2}cos(^{3\theta}/_2)$.

FIG. 1

FIG. 3A

FIG. 2

FIG. 3B

FIG. 3C

FIG. 3D

FIG. 3E

$$V = (2/3) k_I r^{3/2} \cos(3/2\theta)$$

$V = 0$

-V

-V

Insulator

FIG. 4A

AC

22 AWG tube
(electrode &
fluid port)

Observation area

1 mm
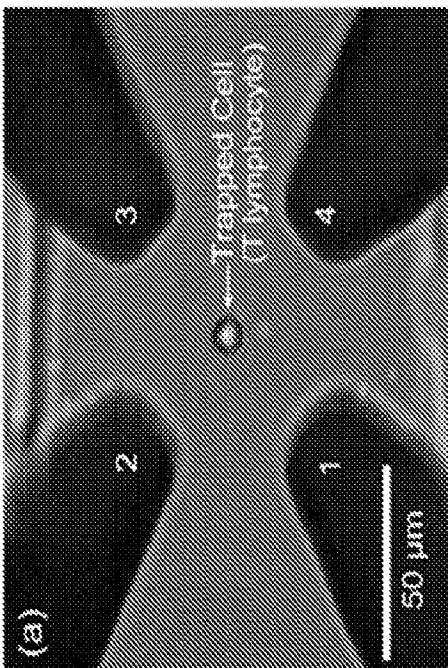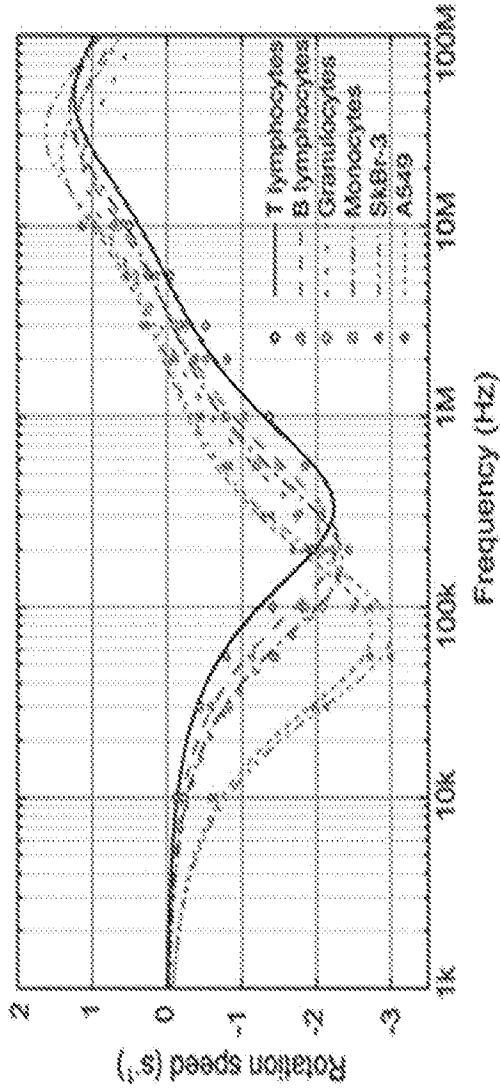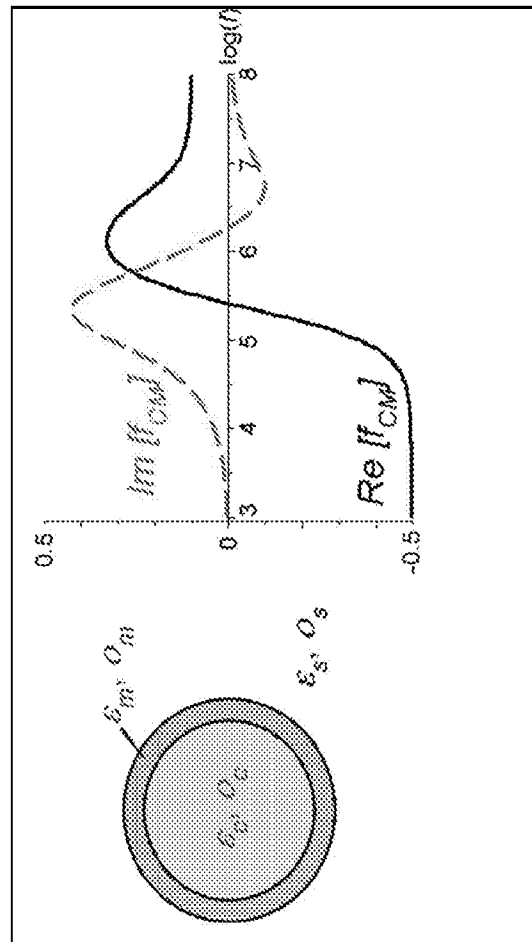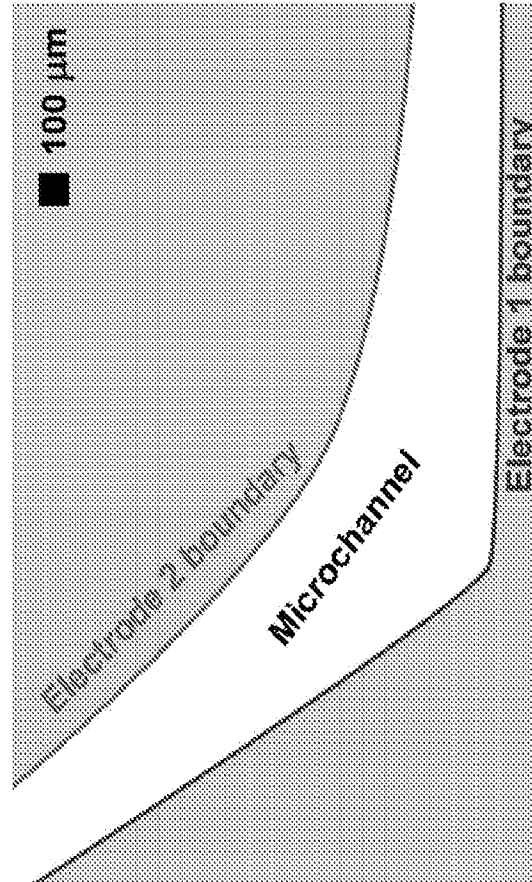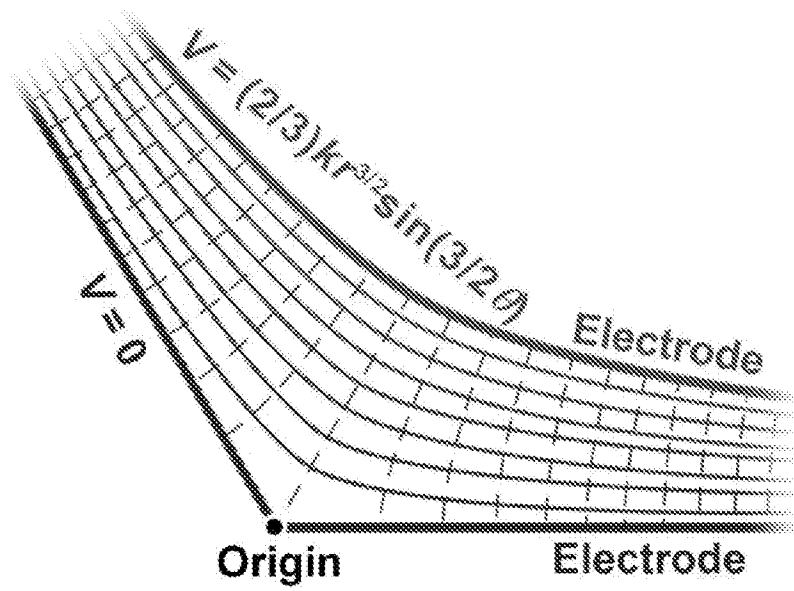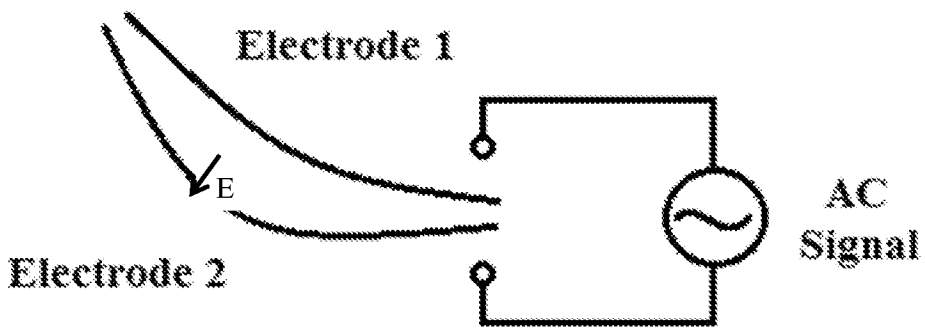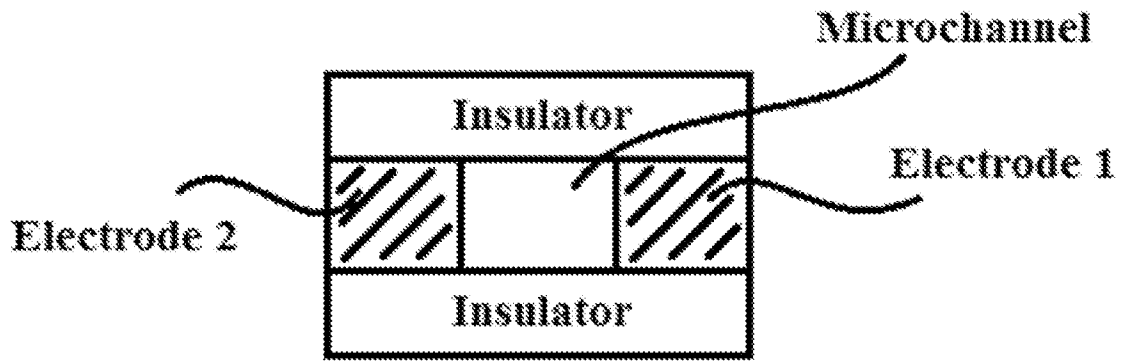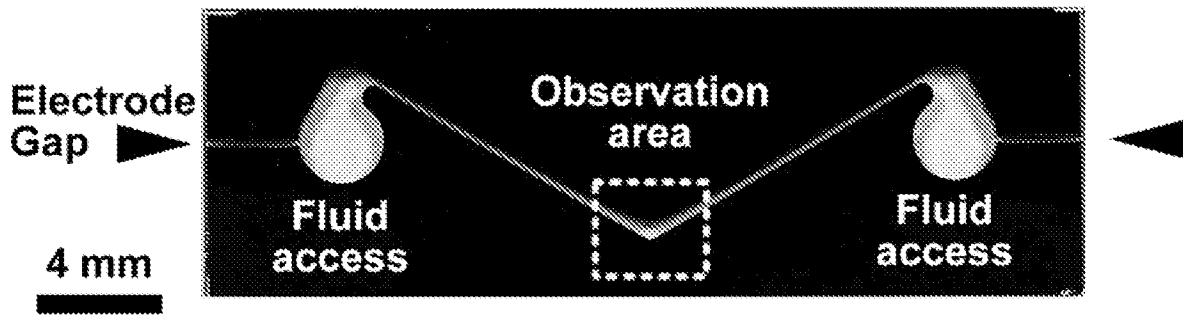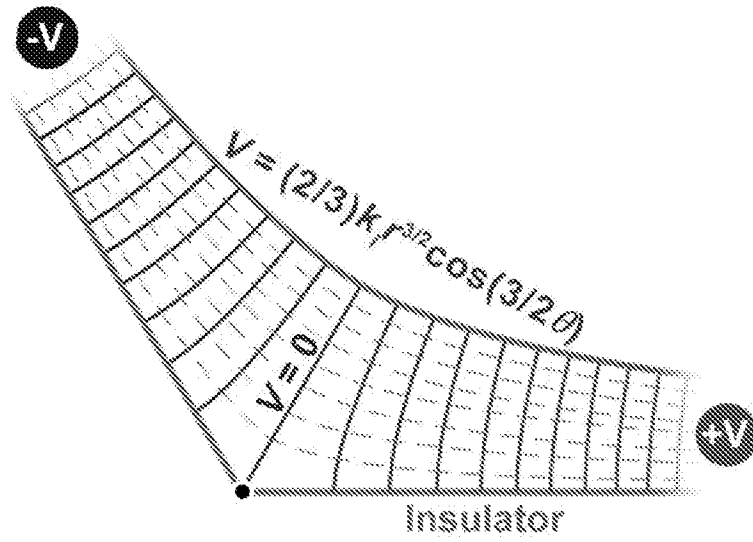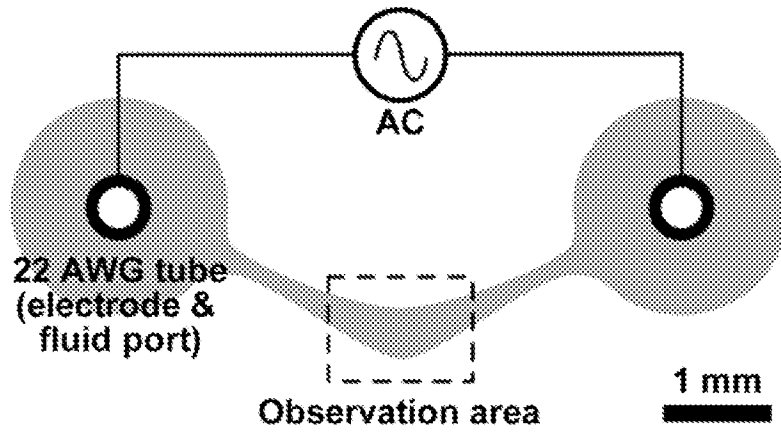
FIG. 4B
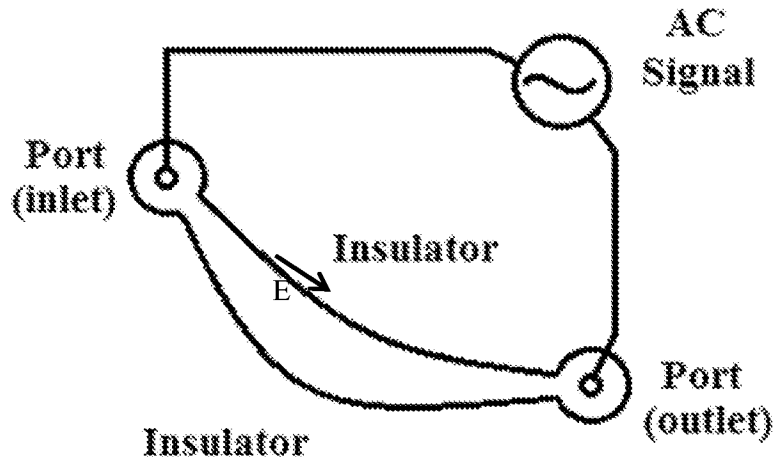
FIG. 4C
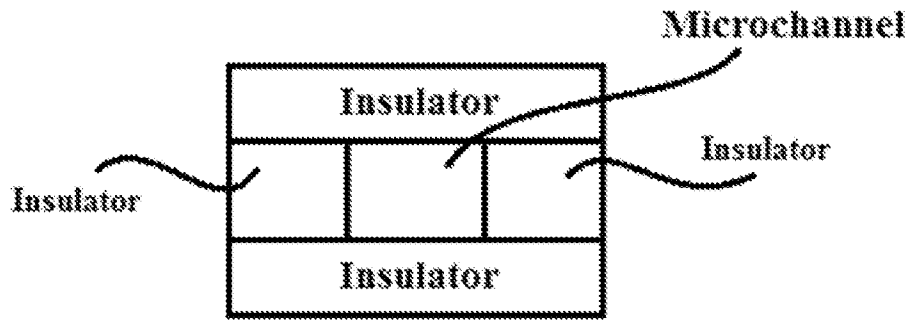
FIG. 4D
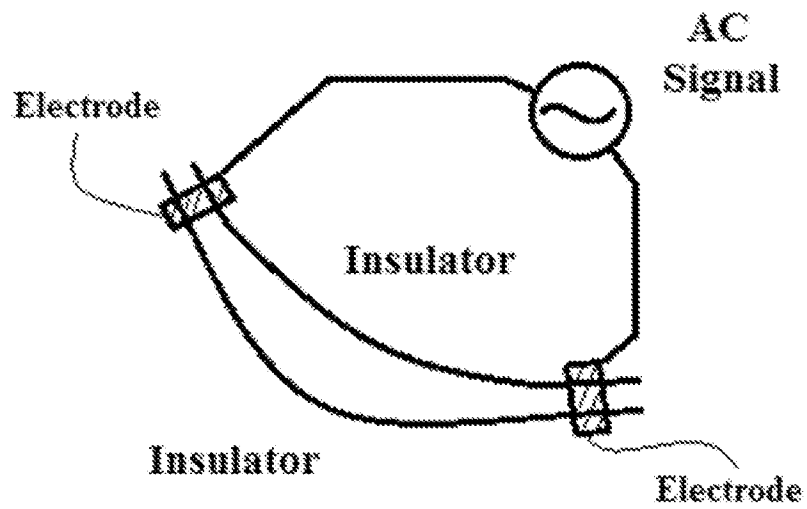
FIG. 4E
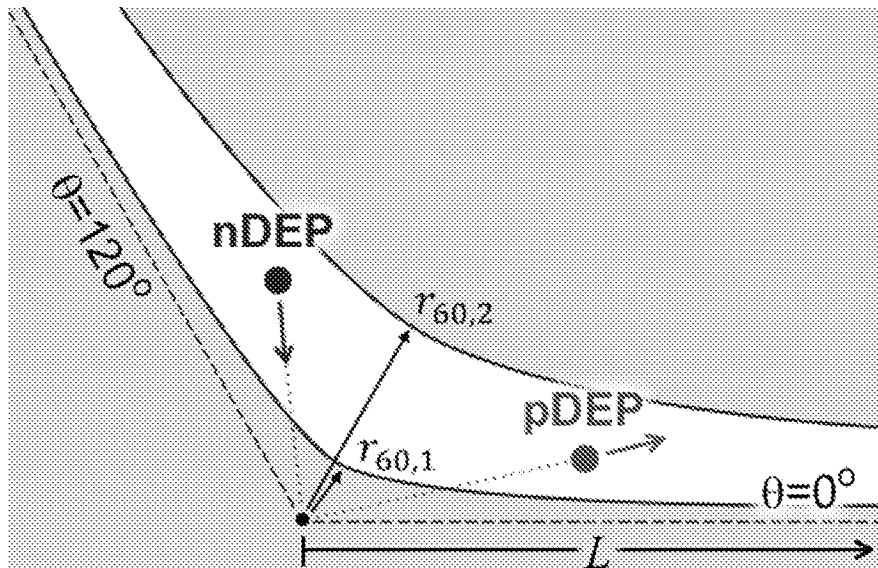
FIG. 5
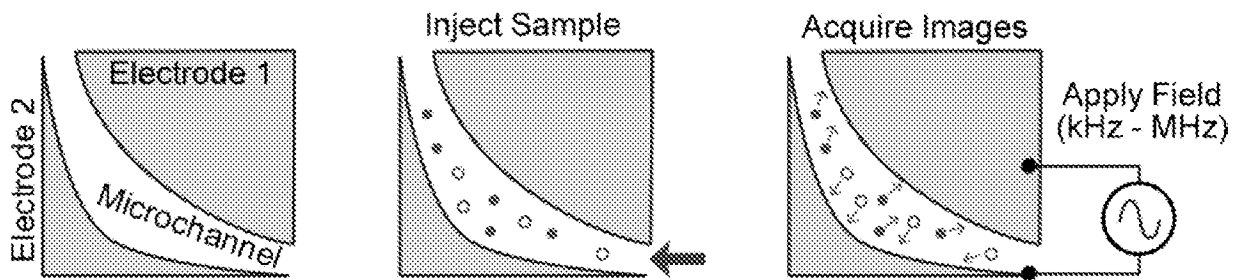
FIG. 6
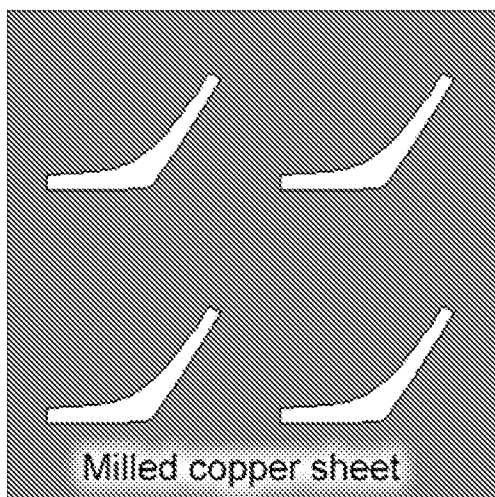
FIG. 7A
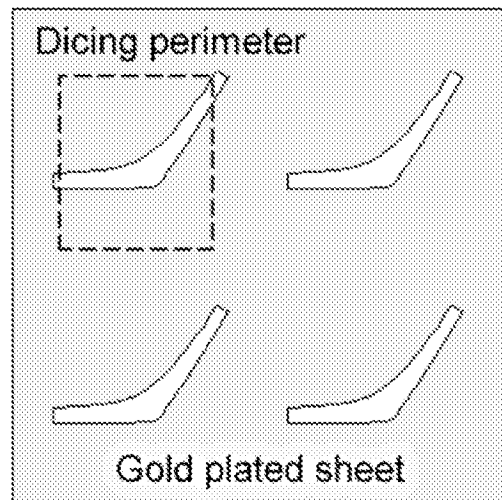
FIG. 7B
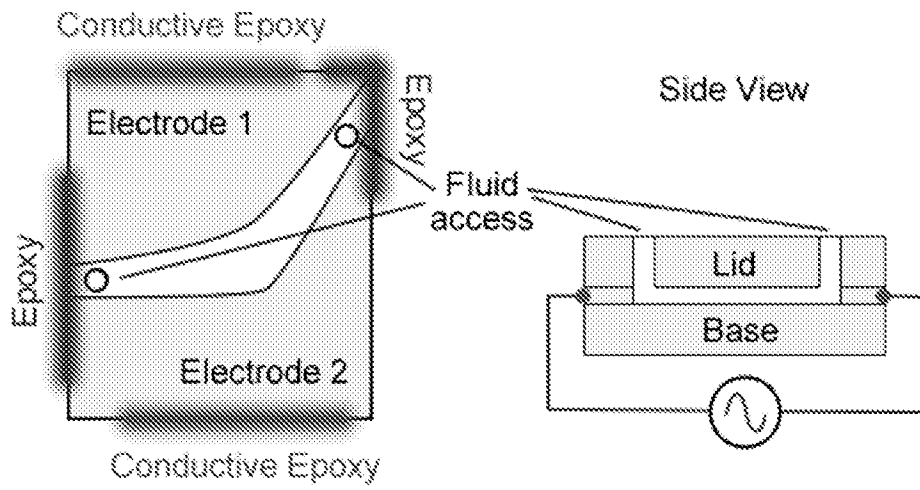
FIG. 7C
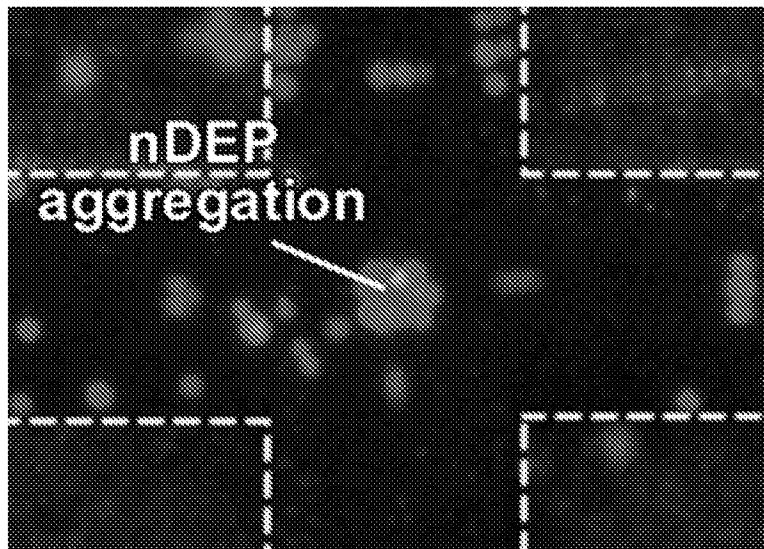
FIG. 8
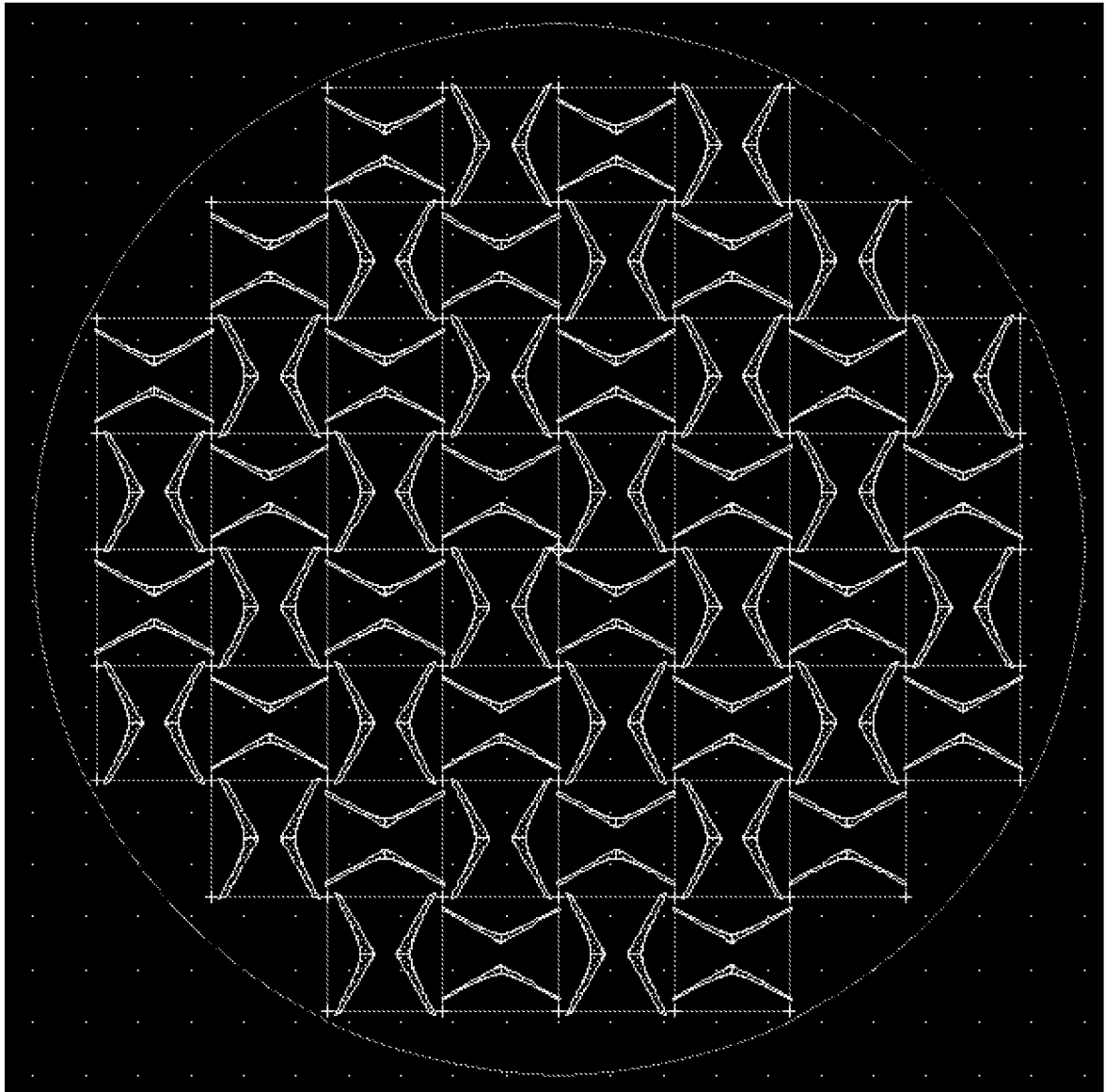
FIG. 9
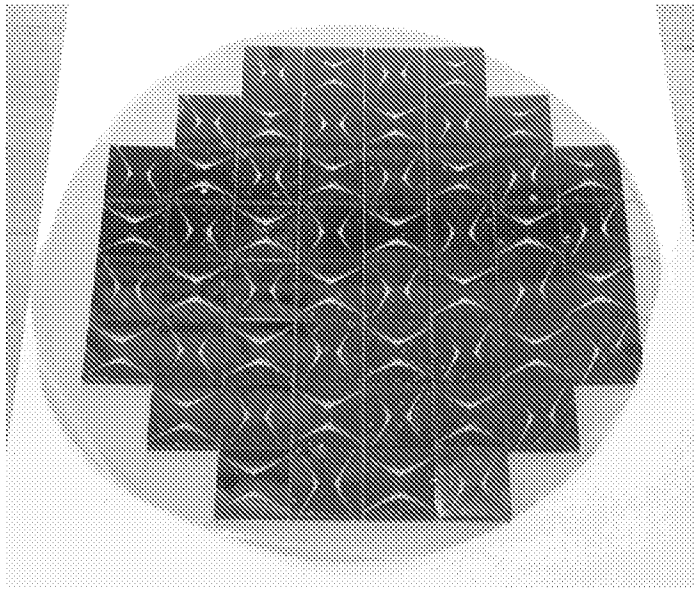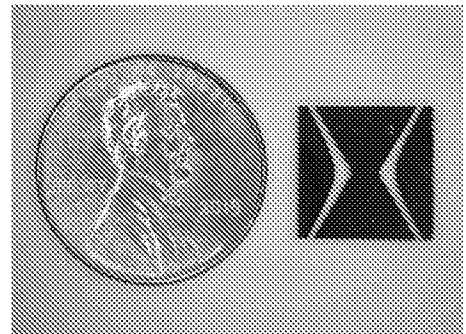
FIG. 10A   FIG. 10B
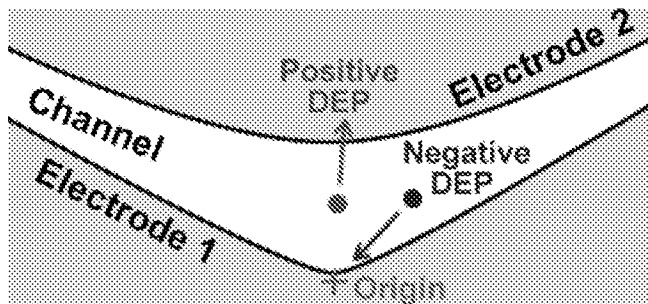
FIG. 11
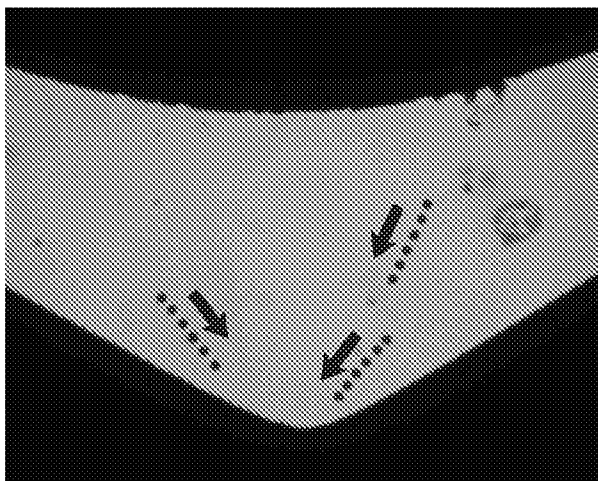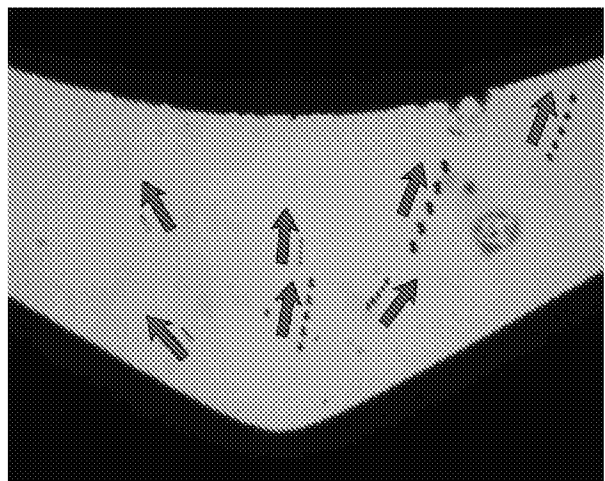
FIG. 12A   FIG. 12B
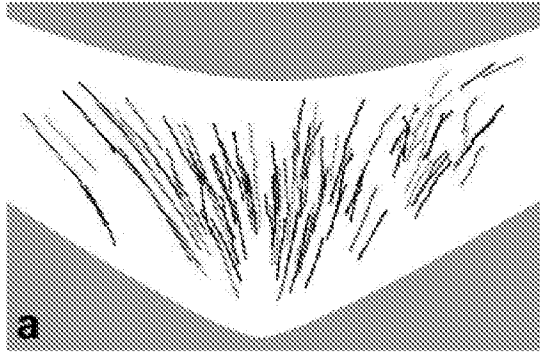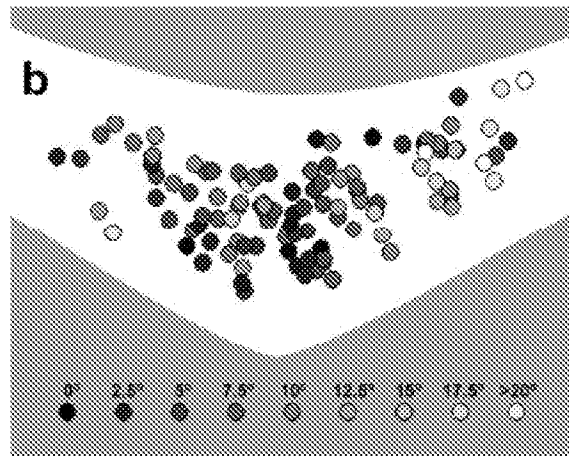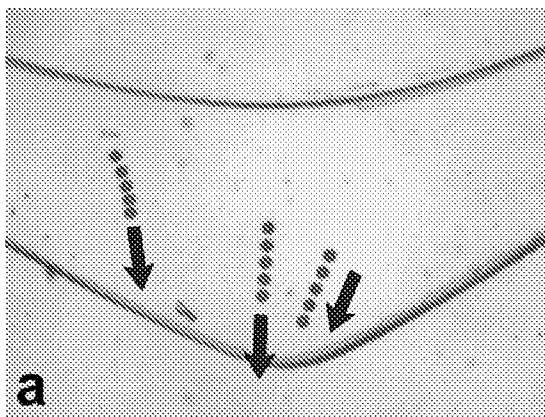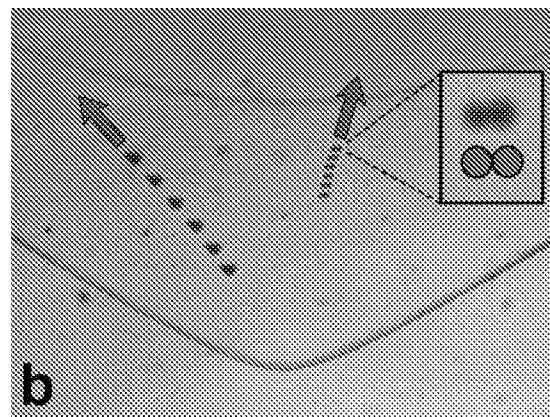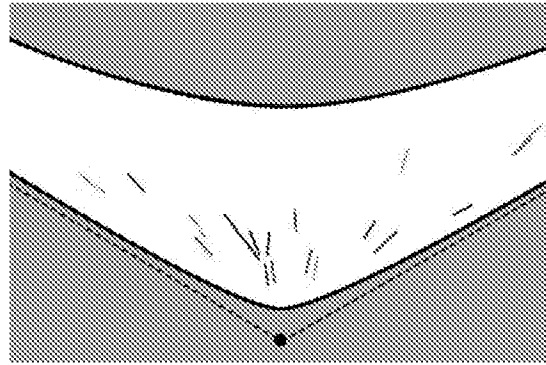
FIG. 13A
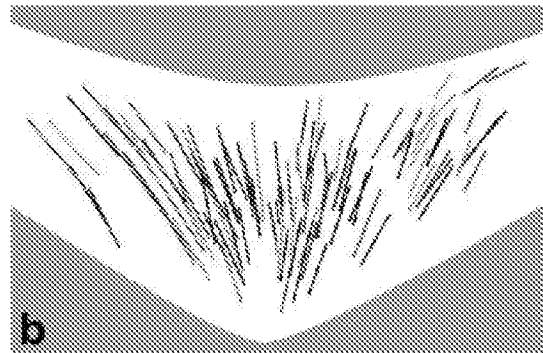
FIG. 13B
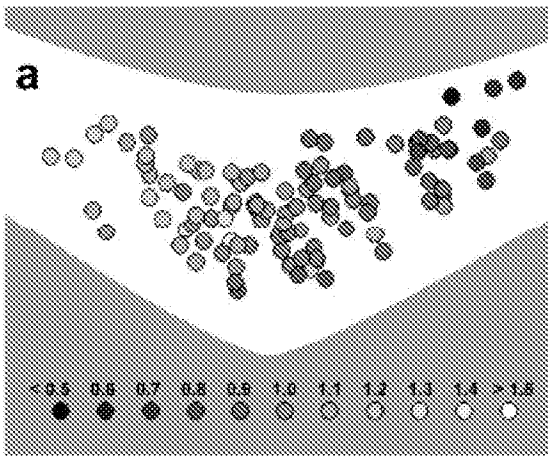
FIG. 14A

FIG. 14B

FIG. 15A

FIG. 15B

FIG. 16

A. CLASSIFICATION OF SUBJECT MATTER
IPC(8) - B03C 5/00, B03C 5/02 (2017.01)
CPC - B03C 5/022, B01 D57/02, B03C 5/026

According to International Patent Classification (IPC) or to both national classification and IPC

B. FIELDS SEARCHED

Minimum documentation searched (classification system followed by classification symbols)

See Search History Document

Documentation searched other than minimum documentation to the extent that such documents are included in the fields searched

See Search History Document

Electronic data base consulted during the international search (name of data base and, where practicable, search terms used)

See Search History Document

C. DOCUMENTS CONSIDERED TO BE RELEVANT

Category*	Citation of document, with indication, where appropriate, of the relevant passages	Relevant to claim No.
X	US 4,326,934 A (POHL) 27 April 1982 (27.04.1982) Col 1 Lines 46-48, 61-64; Col 3 Lines 10-12, 20-23, 30-38, 65-68; Col 4 lines 1-8; Col 5 Lines 23-29; Col 6 Lines 5-10, 43-44; Col 9 Lines 53-61; Col 11 Lines 17-23;	1-9
X -- A	CA 2,238,254 A1 (HARTLEY et al.) 22 November 1999 (22.11.1999) Abstract, Page 2 Lines 33-35; Page 3 Lines 1, 3-4; Page 4 Lines 15-18, 24-27; Page 5 Lines 13-15, 22-24; Page 6 Lines 15-16; Page 27 para[0002], Figures 1, 12	10-14, 16-19 --------- 15, 20
A	ADAPA PROJECT "What is the average size of a cell?" 19 September 2014 (19.09.2014); Page 1 para[0002],[0004] <Retrieved from https://adapaproject.org/bbk_temp/tiki-index.php?page=Leaf%3A+What+is+the+average+size+of+a+cell%3F on 13 September 2017 (13.09.2017)>	12-14, 16-20

☐ Further documents are listed in the continuation of Box C. ☐ See patent family annex.

* Special categories of cited documents:	"T" later document published after the international filing date or priority date and not in conflict with the application but cited to understand the principle or theory underlying the invention
"A" document defining the general state of the art which is not considered to be of particular relevance	
"E" earlier application or patent but published on or after the international filing date	"X" document of particular relevance; the claimed invention cannot be considered novel or cannot be considered to involve an inventive step when the document is taken alone
"L" document which may throw doubts on priority claim(s) or which is cited to establish the publication date of another citation or other special reason (as specified)	"Y" document of particular relevance; the claimed invention cannot be considered to involve an inventive step when the document is combined with one or more other such documents, such combination being obvious to a person skilled in the art
"O" document referring to an oral disclosure, use, exhibition or other means	
"P" document published prior to the international filing date but later than the priority date claimed	"&" document member of the same patent family

Date of the actual completion of the international search	Date of mailing of the international search report
13 September 2017 (13.09.2017)	29 SEP 2017

Name and mailing address of the ISA/US	Authorized officer:
Mail Stop PCT, Attn: ISA/US, Commissioner for Patents P.O. Box 1450, Alexandria, Virginia 22313-1450	Lee W. Young
Facsimile No. 571-273-8300	PCT Helpdesk: 571-272-4300 PCT OSP: 571-272-7774

Form PCT/ISA/210 (second sheet) (January 2015)